VERIFICATION OF PATIENT SPECIFIC QUALITY ASSURANCE SYSTEM FOR VOLUMETRIC MODULATED ARC THERAPY (VMAT)

This thesis / dissertation is submitted to the University of Ghana, Legon in partial fulfilment of the requirement for the award of **MPHIL Medical Physics degree**.

BY

AMOABENG KWAME ANOKYE
(10339761)

OCTOBER, 2020

DECLARATION

This thesis is the result of research work carried out by Amoabeng Kwame Anokye in the Department of Medical Physics, School of Nuclear and Allied Sciences, University of Ghana, under the supervision of Dr. Samuel Nii Adu Tagoe, Dr. Francis Hasford and Prof. Anne Beate Langeland Marthinsen

Sign ……

Amoabeng Kwame Anokye

Date 30/06/2021

Sign ……

Dr. Samuel Nii Adu Tagoe

(Principal Supervisor)

Date 30/06/2021

Sign ……

Dr. Francis Hasford

(Co-supervisor)

Date 30/06/2021

Sign ……

Prof. Anne Beate Langeland Marthinsen

(Co-supervisor)

Date 26/06/2021

DEDICATION

This research work is dedicated to my parents Mr. Daniel Amoabeng and Mrs. Veronica Wiafe and to my siblings.

ACKNOWLEDEMENTS

First of all, I am very grateful to the Almighty Lord for giving me the strength to be able to carry out this research work. A very big thank you to the NORPART PROJECT and the NORPART coordinators both in Ghana and Norway for giving me such a wonderful opportunity to carry out this research work at the St.Olavs Hospital in Norway.

Special thanks to my committed and dedicated supervisors Prof. Anne Beate Langeland Marthinsen (medical physics specialist at the St. Olavs Hospital Trondheim, Norway), Dr Francis Hasford (University of Ghana) and Dr Samuel Nii Adu Tagoe (University of Ghana/ Korle-Bu Teaching Hospital) for sacrificing their time and resources to guide me throughout this project from day one. A very big thank you to the Radiotherapy Department of the St. Olavs Hospital for granting me access to their state-of-the-art equipment and facility for my data collection.

I am also grateful to Dr Gabriel Addio Nketiah (Department of Circulation and Medical Imaging, NTNU) for his encouragement and guidance and for taking me through programming software MATLAB.

I extend my profound appreciation to my parents and siblings; Mr. Daniel Amoabeng, Mrs Veronica Wiafe, Kwabena Baah Amoabeng, Nana Amoako Amoabeng and Priscilla Amoabeng for their support. Finally, a very big thank you to Evelyn Anaafi for her love, support and encouragement in diverse ways.

TABLE OF CONTENTS

LIST OF TABLES

LIST OF FIGURES

ABBREVIATIONS

OAR	Organs at Risk
IMRT	Intensity Modulated Radiotherapy
VMAT	Volumetric Modulated Arc Therapy
MLC	Multileaf Collimators
MU	Monitor Units
QA	Quality Assurance
2D	Two Dimensional
3D	Three Dimensional
TPS	Treatment Planning System
FIGO	International Federation of Gynecology and Obstetrics
FFFB	Flattening Filter Free Beam
FB	Flattened Beam
HPV	Human Papilloma Virus
CT	Computed Tomography
MRI	Magnetic Resonance Imaging
EBRT	External Beam Radiation Therapy
CTV	Clinical Target Volume

CRT	Conformal Radiotherapy
DAO	Direct Aperture Optimization
IGBT	Image Guided Brachytherapy
ICRU	International Commission on Radiation Units and Measurement
LINAC	Linear Accelerator
SAD	Sources to Axis Distance
PTV	Planning Target Volume
DTA	Distance to Agreement
DD	Dose Deviation
PDD	Percentage Depth Dose
CI	Conformity Index
HI	Homogeneity Index
NTNU	Norwegian University of Science and Technology
PMMA	Polymethylmethacrylate

ABSTRACT

Background: Volumetric Modulated Arc Therapy (VMAT) plans and its treatment are complex modalities and its clinical implementation requires very accurate acceptance testing and a very comprehensive quality assurance program. Failure in their periodic applications can result in errors in treatment delivery. There is therefore the need to compare the calculated dose distribution to the measured dose distribution of treatment plans to ensure accuracy, efficiency and minimize errors in planned radiation dose delivery to the patient.

Methods: 15 patients with pathological pelvic lymph node metastasis were included in this study. Measurements were done using both conventional 6 MV beam with flattening filter and flattening filter free beam (FFF) for all 30 VMAT plans. Each patient thus had a 6 MV plan and an FFF plan. The treatment plans were made using two arcs and then delivered to the delta4 phantom. All 30 VMAT plans were replicated on the Delta4 phantom using three Elekta linear accelerators.

Results: After machine optimization, there was an increase in the mean total gamma pass rate for the 6 MV plans from 98.7 to 99.9% and the FFF plans also had an increase in the gamma pass rate from 91.7% to 98.4%. There was significant statistical difference between the pass rates of the 6 MV plans and the FFF plans ($p = 0.000488$). The total monitor units (MUs) for the FFF plans were significantly greater than the 6 MV plans ($p = 6.1 \times 10^{-5}$).

Conclusion: 6 MV VMAT plans with conventional flattened beams are delivered more accurately and hence more beneficial compared to flattening filter free (FFF) VMAT plans for external radiation of cervical cancer with affected pelvic lymph nodes.

CHAPTER ONE

1 INTRODUCTION

1.1 BACKGROUND

The primary aim of radiotherapy is to deliver an optimal dose to the target volume whilst minimizing the dose to the organs at risk (OAR). Advancements in technology have allowed for more accurate and precise treatment making radiotherapy a feasible option as a cure for individuals diagnosed with cancer. Radiation alone or concurrent chemoradiation results in significant improvements in tumor cure rates. To illustrate this, scientists conducted a study with gastric cancer patients. It was revealed that radiation combined with chemotherapy resulted in a better survival rate than treating with chemotherapy alone (Abshire and Lang, 2018). In order to get a three-dimensional representation of a patient from a CT scanner, it is necessary to image multiple slices.

Intensity modulated radiotherapy (IMRT) allows highly conformal non-convex dose distributions. Volumetric modulated arc therapy (VMAT) is an arc delivery technique which is delivered by means of one or more linac gantry rotations. VMAT is one of the state-of-the-art techniques in radiation therapy. VMAT delivery involves changing in multileaf collimators (MLCs) with varying dose rate and gantry speed and allows high dose conformity and sparing of normal tissues while significantly reducing the number of monitor units (MUs) and the delivery times (Allison, 2013). According to (Hoffmann et al., 2019) a leading source of concern associated with using VMAT is the potential increase

in low dose radiation to the surrounding normal tissues which could increase the risk of complications and result in secondary malignancies. However, some dosimetric planning studies have demonstrated higher sparing to organs at risk with VMAT compared to IMRT (Yoo, 2010). VMAT treatment usually involves diagnosis, treatment planning and delivery. As part of the diagnosis, the oncology team generates three-dimensional images of the patient's anatomy and then uses these images to determine a treatment plan.

The quality assurance (QA) burden related with the implementation of VMAT has been considerable and that verification processes play a vital role in the extent to which a center can provide quality radiotherapy services (Abolaban et al., 2016). Volumetric errors according to (Dixon and O'Sullivan, 2002) result from poor decisions made during the treatment planning, treatment set-up variation or organ motion during or between fractions. An issue of increasing importance is the growing body of knowledge concerning inter-fraction isocenter and target organ movement. Each step in the radiotherapy process could generate erroneous data (simulator, treatment planning system, record and verify, treatment unit) and transfer of data could equally be prone to errors. Depending on the available equipment, the generation and transfer of information as well as errors will differ between departments. The growing complexity of the radiotherapy process suggests an increased probability of inaccuracy and accidents and requires the development improved control mechanisms to ensure optimal treatment quality (Esch et al., 2000).

All VMAT plans require a dedicated QA procedure verification of the planned dose distribution to check for the agreement between the dose distribution calculated by the treatment planning system (TPS) and the corresponding measured dose distribution as reported by (Natali et al., 2016). It is therefore crucial to ensure that the delivery system

can deliver modulated beams with allowable precision considering the performance of the MLC and the linear accelerator.

Cervical cancer is the second most common cancer and the fifth leading cause of cancer-related deaths in women worldwide (Zivanovic et al., 2008). Currently, the treatment modalities for locally advanced cervical cancer consist of external beam radiation therapy (EBRT) with concurrent chemotherapy which is followed by intracavitary brachytherapy.

Gamma analysis has become the mainstay for patient specific quality control for IMRT and VMAT. As stated by (Agnew and McGarry, 2016), gamma analysis has become a tool to assess the accuracy of large volumes of patient specific treatment deliveries which combines spatial information and dose differences for a two dimensional (2D) plane or a three dimensional (3D) volume. The agreement between the planned and measured dose distribution may be affected by both the accuracy of the treatment planning system calculation and the delivery accuracy. The dose inside an inhomogeneity is difficult to calculate, but the effect of an inhomogeneity on the dose beyond the inhomogeneity is comparatively simple to measure and quantify. Treatment time and MU calculations form an important aspect of the radiation dose delivery process and the data on treatment time and MU are usually provided by the TPS after passing the dose prescription procedure (Han et al., 2018). It is important to verify that the given dose distribution can be verified as planned.

1.2 STATEMENT OF PROBLEM

Volumetric modulated arc therapy is a development of intensity modulated radiation therapy that has many advantages in the delivery of the radiation beam for various tumor sites including the cervix. The gantry speed, multileaf collimator speed and the dose rates are varied in VMAT. The combination of 3D planning and variable radiation intensity provides dosimetric advantages which have been utilized in a variety of pathologic sites including cancer of the cervix. Cervical cancer management varies depending on the International Federation of Gynecology and Obstetrics (FIGO) stage, but radiotherapy plays a critical role across the range of presentations (Hartford, 2012).

Patient specific QA is a core element of the quality assurance procedure which is emphasized by most professional institutions including the American Association of Physicists in Medicine (AAPM), American College of Radiology (ACR) and the American Society for Radiation Oncology (ASTRO) (Hartford, 2012).

Pre-treatment quality assurance programs for the safe delivery of patients' treatments and QA method for dynamic dose delivery by phantom measurements have been proposed in literature (Ma et al., 2003). Both VMAT plans and its treatment are complex modalities and its clinical implementation requires very accurate acceptance testing, commissioning of delivery and treatment planning system and a very comprehensive quality assurance program. According to (AAPM, 2009), there is evidence that VMAT plans may not always be accurate. Inadequate patient specific quality assurance (QA) program and failure in their periodic applications can result in errors in treatment delivery. There is therefore the need to compare the calculated dose distribution to the measured dose distribution of treatment

plans to ensure accuracy, efficiency and minimize errors in planned radiation dose delivery to the patient. The gamma index which was introduced by (D. A. Low et al., 1998) is used to quantify the agreement between the measured dose distribution and the calculated dose distribution.

1.3 OBJECTIVES

The aims of this study are to verify patient specific quality assurance system of volumetric modulated arc therapy and to determine if flattening filter free radiation (FFF) plans and 6 MV made for the same patient are being delivered with the same accuracy and to evaluate differences in delivery accuracy between linacs and also within one linac before and after a VMAT optimization.

The specific objectives of this study;

- To evaluate 3D gamma index before and after VMAT optimization of the linear accelerators.
- To determine if flattening filter-free (FFF) plans and 6MV plans are being delivered with the same accuracy.
- To verify if patient specific treatment plans are technically feasible.

1.4 RELEVANCE AND JUSTIFICATION

Verification of patient-specific QA in VMAT would ensure that the treatment plan delivered to the patient is an accurate representation of the calculated plan. This would help to determine if a treatment plan could be administered to the patient. That is if the plan meets the passing criteria or not. For patients with lymph node metastasis, this study would help to determine the accuracy of delivered dose for different linacs and for the same linac before and after MLC calibration. This would provide possibilities to develop acceptable plans with flattening filter free photon beams and explore their potential benefits to cervical cancer patients.

1.5 ORGANIZATION OF THESIS

Chapter one consists of the background of the study, the statement of the problem, the purpose of the study and the research objectives. Chapter two would contain literature which is relevant to the scope of study. Chapter three would cover the methodology of the study. This chapter would describe the methods and materials used for the study. Details on how the patient specific QA is performed on the linear accelerator using the Delta^4 phantom would be specified. In Chapter 4, the results from the QA procedure would be presented and discussed. Chapter five would present the summary, conclusion, as well as recommendations to relevant stakeholders.

CHAPTER 2

2 LITERATURE REVIEW

2.1 INTRODUCTION

This section covers relevant literature on cervical cancer, external beam radiation therapy, intensity modulated radiotherapy and volumetric modulated arc therapy, cervical cancer, quality assurance, delta^4 phantom, multileaf collimators, treatment planning system, gamma index, monitor unit, flattening filter and filter free radiation, EMBRACE studies, homogeneity and conformity indices.

2.2 CERVICAL CANCER

The cervix is in the lower part of the uterus and usually 2 to 3 cm long and cylindrical in shape which changes shape during pregnancy. The narrow, central cervical canal runs along its entire length connecting the uterine cavity and the lumen of the vagina. The opening of the uterus is called the internal os and the opening into the vaginal is called the external os (Hata et al., 2013). The cervical canal is lined with a single layer of column shaped cells while the ectocervix is covered with multiple layers of cells topped with flat cells. The two types of epithelia meet the squamocolumnar junction. Infection with the human papillomavirus (HPV) can cause changes in the epithelium which can lead to cancer of the cervix. Part of the lining of the cervix contains glands that make and release mucus.

This mucus helps to protect the uterus and upper female reproductive organs from harmful bacteria.

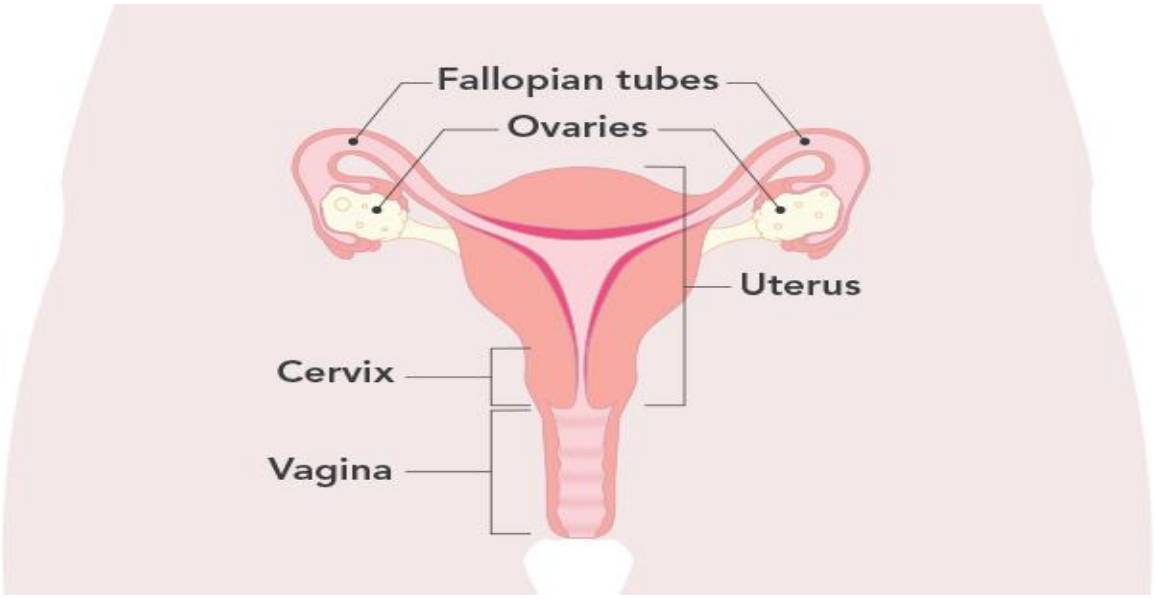

Figure 2.1: Anatomy of the female reproductive system showing the location of the cervix (Cohen et al., 2019).

The Federation of Gynecology and Obstetrics (FIGO) system is used to determine the stage of a cervical cancer depending on the characteristics of the cancer. There are four main stages of cervical cancer and it includes; stage I (where the cancerous area is less than 3mm in depth), stage II (the cancer has spread beyond the uterus to nearby areas such as the vagina or tissue near the cervix but it is still in the pelvic area), stage III (where the tumor involves the lower third of the vagina and has spread to the pelvic side wall causing swelling of the kidney and involves regional lymph nodes) and stage IV (the cancer has spread to the bladder or rectum but it has not spread to other parts of the body). With stage IVB, the cancer has spread to other parts of the body (Pecorelli and 2009).

Cervical cancer is the fourth most common female malignancy worldwide and represents a global health challenge (Cohen et al., 2019). High-risk subtypes of the human papillomavirus (HPV) causes almost all cervix cancers and HPV screening and vaccination are effective in disease prevention (Hata et al., 2013). Squamous cell carcinoma and adenocarcinoma of the cervix represents approximately 70% and 25% of all cervical cancers (Small et al., 2017).

Cervical cancer treatment can be curative (radical) or palliative. Radiation therapy plays an important role in the treatment of cervical cancer which comprises EBRT and intracavitary brachytherapy using a 3D approach based on CT/MRI. Radical radiotherapy combines EBRT to the pelvis with concomitant cisplatin chemotherapy followed by intracavitary brachytherapy (Small et al., 2017). The choice of a treatment modality is based on institutional practice, radiation oncologists involved and the general health of the patient. Studies have suggested that the 5 year overall survival of cervical cancers could decrease by almost 30% as lymph node metastasis occurs (Hata et al., 2013).

For patients with early-stage cervical cancer, lymph nodes metastasis is a critical factor related to their survival (Bats et al., 2011). Patients with positive nodes, parametrial invasion or positive vaginal margin are at a high risk of recurrence. It was reported by (Li et al., 2013) that patients who had concurrent cisplatin with pelvic radiotherapy also suffered from treatment toxicities. The medial external iliac and obturator nodes are the most common areas for metastases (Liu et al., 2016). The conformal dose distributions and the dose gradients generated around the target volumes created by VMAT planning needs accurate treatment setup and constant monitoring to prevent geographical misses during radiotherapy.

In conventional treatment, EBRT is delivered with either anterior and posterior fields or the box technique and this reduces high dose volume. Bowel complications reduced from 17.5 to 2.9% using box technique and lymphoedema from 28.6 to 3.1% (Yamazaki et al., 2000). The planning target volume margin around the cervix and uterus is dependent on internal motion and the margin around the less mobile CTV is defined by the set-up error. In patients with recurrent pelvic disease, after hysterectomy, brachytherapy may not be possible (Du et al., 2018). Accurate target-volume delineation and 3D planning techniques for cervical cancer improves outcomes by ensuring enough target coverage and reducing doses to the organs at risk. The Federation of Gynecology and Obstetrics (FIGO) system is used to determine the stage of a cervical cancer depending on the characteristics of the cancer (Hartford, 2012).

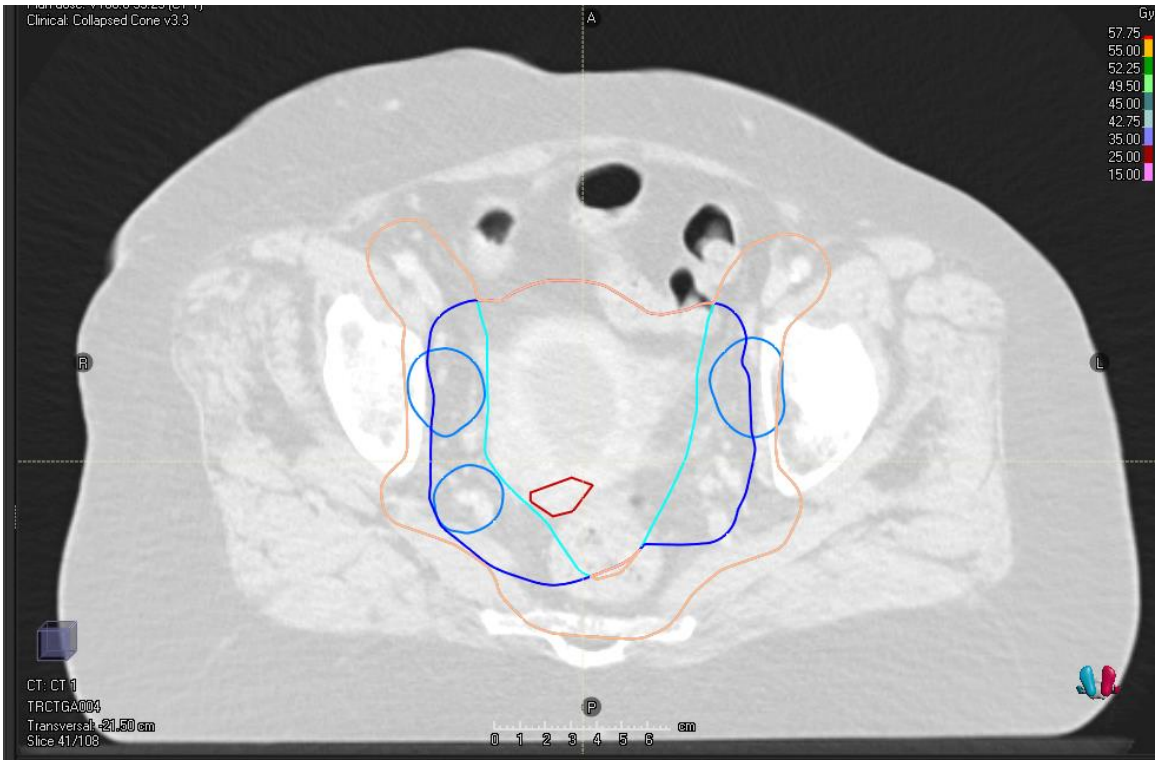

Figure 2.2: A VMAT plan showing the PTV_45 union on the treatment planning system.

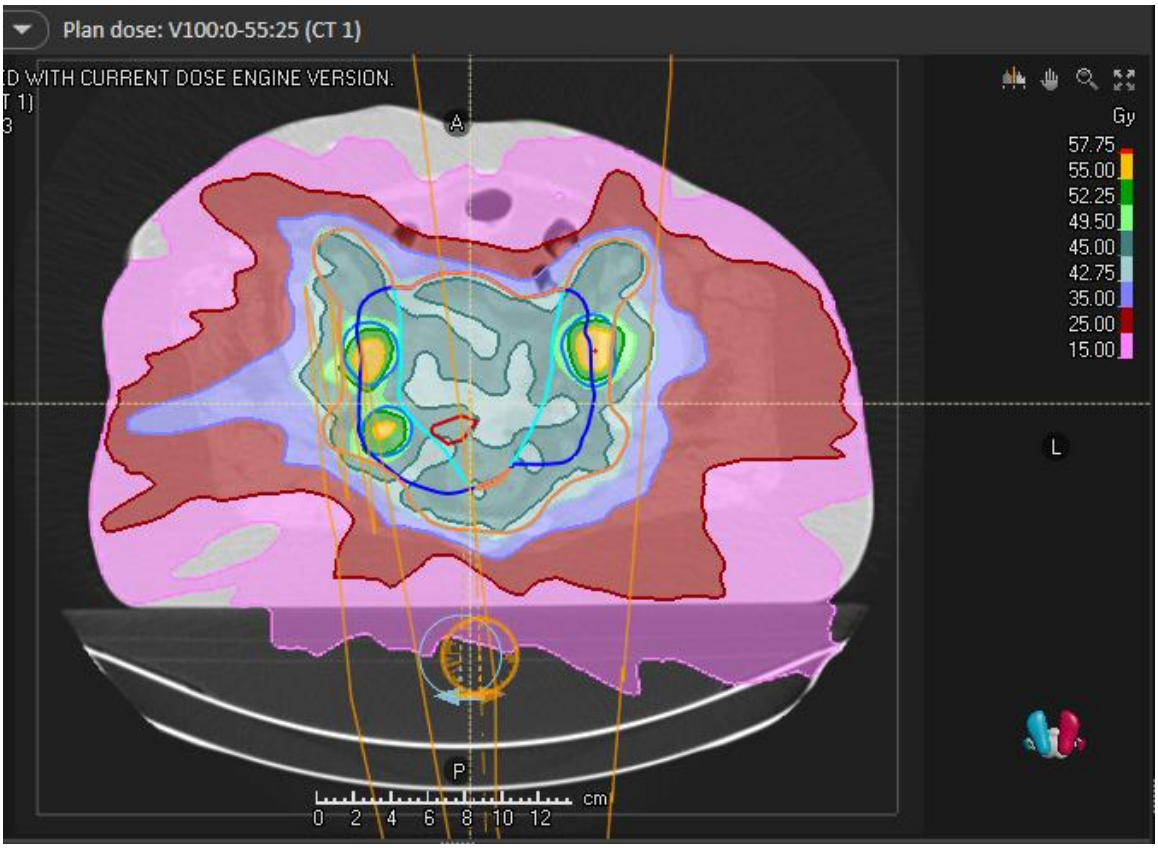

Figure 2.3: A cervical cancer VMAT plan generated by the Raystation TPS showing delineated pelvic lymph nodes and dose distribution.

2.3 EXTERNAL BEAM RADIATION THERAPY

External beam radiation therapy (EBRT) is a treatment modality which involves the use of high energy (photons, electrons, particles) ionizing radiation to kill tumor cells. It began after the discovery of X-rays in 1895 and radioactivity in 1896. EBRT started with superficial and orthovoltage treatment which used x-ray tubes. The betatron and microtron have also previously been used in radiation therapy (Thwaites and Tuohy, 2006). As technology developed over the years, there was an advent of 2D imaging technique. This

uses X-ray images of the patient to localize the tumors and avoid or reduce the radiation doses to the various organs at risk. The radiation beams are produced at a distance away from the patient by either a Cobalt -60 teletherapy unit or a linear accelerator. Improved computer imaging has provided better 3D treatment planning techniques and a better definition and delineation of the target volume and organs at risk.

The various beam energies used for EBRT are 1.25 MV for Co-60, 6-15 MV for megavoltage X-rays and 6-18 MeV for clinical electron beams. EBRT is used for either curative or palliative intent. The medical or radiation oncologist contours the target volumes using computed tomography images of the patient and the organs at risk and prescribes the radiation dose. Although Co-60 treatment is being phased out, it still useful for the treatment of various tumors in some countries since it is relatively reliable and less expensive to maintain when compared to the linear accelerator. The source-to-axial distance (SAD) for treatment machines are either 80 cm or 100 cm. Radiation therapy can be combined with chemotherapy or surgery to produce better treatment outcomes (Abshire and Lang, 2018).

The use of CT images is suboptimal in terms of volume definition. The delineation of the prostatic apex on CT presents some difficulties because it is limited by the soft tissue contrast between the apex itself and the muscles of the pelvic floor. To overcome this, magnetic resonance imaging (MRI) have been introduced in the planning process to improve the localization accuracy (Chen et al., 2006). MRI provides images which has excellent spatial resolution to better characterize soft tissue compared to CT and its implementation in designing treatment plans is now possible with the availability of computer algorithms (Sannazzari et al., 2002).

For improved tumor delineation and treatment, IMRT, VMAT, image guided radiotherapy (a delivery technique which enables localization and tracking of tumors in real time of treatment delivery and make necessary adjustments whenever the tumor moves outside the treated volume), stereotactic body radiotherapy, stereotactic radiosurgery, cone beam computed tomography (a technology using multiple X-rays from different angles that are merged by the computer to generate a 3D image to verify patient position before treatment) are currently in use (Troost et al., 2015).

2.4 IMRT AND VMAT

Tumors usually assume very complex shapes and tumor volumes may present with varying concentrations of cancerous cells. These, coupled with patient's surface contour along irradiated region, would require the modulation of fluences of beams to be used for treatment to be able to conform the dose distribution to the tumor. Thus, reducing doses to normal tissues in close proximity to the tumor and escalate doses to areas of the tumor with very high concentration of cancerous cells. Treatment modalities have been introduced to achieve beam intensity modulation during treatment delivery and these are Intensity Modulated Arc Therapy (IMRT) which is based on fluence optimization and Volumetric Modulated Arc Therapy (VMAT) which is based on aperture optimization.

IMRT is a treatment delivery technique that divides each individual beam into beamlets using multi-leaf collimators (MLC's). The irradiation is done with very many individual segments from defined gantry angles and there is no radiation when the gantry moves (Marcu et al., 2012). Cedric Yu developed IMRT in 1995 and the idea was to deliver plans with many gantry

positions. The fluence map of the beam is pre-calculated and decomposed to several apertures. These apertures are delivered at a gantry position by multiple segments (Yu and Tang, 2011). IMRT requires more segments which extends treatment time. There is non-uniform intensity inside the treatment field to achieve optimum dose distribution. This improves dose conformity to the target volume and reduces dose inhomogeneities in off-axis slices. Advantages of IMRT include better normal tissue sparing, better conformality, superior dose distribution when compared to 3D conformal radiotherapy, dose escalation possibilities and more target-tailored plans (Cihoric et al., 2015). IMRT provides highly conformal dose distributions around the planning target volume and allows delivery of a high dose within a single fraction and eliminates the complexity of multiple fractions of treatment with 3D-CRT to deliver this dose using photon field matching. This conformity reduces dose to the organs at risk thus reduces the toxicity experienced (Hoskin et al., 2006). In IMRT, each beam is broken into smaller beamlets where some beams are stronger than others which gives a desired dose distribution.

Concave dose distributions in IMRT results in target doses that are not uniform. IMRT plan processes include; localization and image transfer, contouring, beam definition, dose calculation and plan evaluation. It was reported by (Kung et al., 2001), that comparing 6-field 18 MV 3D-CRT plans and 9-field 6 MV IMRT plans for three cases indicated that the IMRT plans had greater tissue sparing for the bladder and rectum for prostate radiotherapy. Intensity-modulated radiotherapy represents an improvement in 3D conformal radiotherapy since the target volume and organs at risk are outlined on the volumetric computer tomography data set used for treatment planning. These structures are assigned dose and volume constraints and an inverse planning treatment planning system generates a combination of beams of non-uniform intensity. IMRT generates more conformal dose distributions with sharp dose gradients that potentially facilitate enhanced organ at risk sparing compared with 3D conformal radiotherapy

(Palisca et al., 2009). Multileaf collimators can be adjusted during treatment to deliver radiation beams with non-uniform intensity.

VMAT is an advanced/improved technique for intensity modulated radiation therapy where the gantry rotates around the patient with dynamic changes of radiation beam shape and intensity by multileaf collimators and change in dose rate and gantry speed. VMAT helps to focus the radiation on the tumor volume and protects healthy tissues (Otto et al., 2011). According to (Cihoric et al., 2015), VMAT treatment received approval by the US Food and Drug Administration in 2008 and studies have compared plan quality, delivery efficiency and accuracy of VMAT delivery to other treatment techniques like three-dimensional conformal radiotherapy (3D CRT), IMRT and tomotherapy. VMAT maximizes the benefit of IMRT by treating with the widest range of beam orientations within a short treatment time. Most treatment planning systems provide VMAT optimization function and rely on the Direct Aperture Optimization (DAO) algorithm and this handles the complexity of VMAT optimization using stochastic approach (Onizuka et al., 2018).

It was concluded by (Verbakel et al., 2009) who sought to determine if VMAT was beneficial for patients undergoing radiotherapy to the head and neck that one arc VMAT plans for both conformity and homogeneity were inferior to IMRT. However, this effect is not seen when using two arcs for VMAT. Conformity for VMAT plans were found to be a little less than IMRT plans. This difference didn't exhibit any clinical effect. Homogeneity increased in VMAT plans which could have a positive impact on tumor control. Although there was a variation in results for organs at risk, none of them found the VMAT plans to be inferior to IMRT. Several treatment planning studies have demonstrated the potential of VMAT to deliver plans with a quality comparable to IMRT in shorter treatment time. The procedures for VMAT

specific commissioning and quality assurance of linear accelerators to ensure synchronization of the simultaneously varying parameters have been proposed by (Ling et al., 2008).

VMAT is a useful technique for treating large mediastinal Hodgkin's lymphoma and allows maximal heart and lungs sparing when compared to 3D CRT in some selected Hodgkin lymphoma patients treated with Involved Site Radiation Therapy (ISRT). The issue of concern with the use VMAT is the spreading of low radiation doses to normal tissues and hence an increased integral dose (Higby et al., 2016). It was reported by (Holt et al., 2011) that coplanar VMAT for stereotactic body radiation therapy for early-stage lung cancer produced a plan quality and skin dose levels which is similar to those using noncoplanar IMRT and slightly better than those with coplanar IMRT. In addition, the delivery time could be reduced by 70% with VMAT. Different treatment planning and delivery solutions for VMAT have been developed by different vendors including Rapid Arc by Varian, VMAT by Elekta and SmartArc by Philips Medical Systems.

VMAT technology compared to IMRT further reduces treatment time and the number of MU without affecting the dose distribution to improve the treatment target of biological effects and the number of patients treated in a unit of time. Reducing the number of monitor units reduces the number of scattering lines of the collimator (Shaffer et al., 2009). Eventually, this improves the accuracy of dose distribution and treatment effect. The process of dose designing and optimization of IMRT and VMAT plans takes longer time than that of 3D-CRT because the parameters are adjusted and optimized repeatedly. Optimization of VMAT plans is divided into several steps and because of many physical parameters in the optimization plan, the process is complex and limited to the version of the system (Qiu et al., 2010).

2.5 EMBRACE STUDIES

Conventionally, treatment of locally advanced cervical cancer includes external beam radiation therapy, concomitant chemotherapy and brachytherapy where doses have been prescribed to Point A according to the Manchester system (Serban et al., 2018). Duration of the irradiation was based on the dose rate to Point A which is located 2cm superior to the cervical orifice and 2cm lateral to the cervical canal. The GEC ESTRO GYN group started working in 2000 and was tasked to support and modify image guided gynecologic brachytherapy (IGBT) based on European centers involved in image guided treatment and to develop prognostic and predictive statistical models for clinical outcome including volumetric, dosimetric, clinical and biological risk factors (Tan et al., 2018). The Gec Estro Gyn Network made recommendations on contouring tumor target and organs at risk (OAR) and dose volume parameters to be reported for image guided brachytherapy for locally advanced cervical cancer (Pötter et al., 2005).

As a major advantage of this technique, there is the possibility to conform the dose given by brachytherapy regarding both volume (3D) and (4D). Through repetitive imaging before each brachytherapy implant, it is possible to adapt the dose given by brachytherapy to the anatomy of each patient taking into account the tumor regression which is often obtained by preceding EBRT and chemotherapy (Berger et al., 2019). The recommendations of GEC ESTRO GYN have been used for the implementation of image guided adaptive brachytherapy (IGABT) worldwide and are entrenched into the International Commission on Radiation Units and Measurements (ICRU) report 89 (Berger et al., 2019). Patients with squamous carcinoma, adenocarcinoma of the uterine cervix, FIGO stage IB, IIA, IIB, IIIA, IIIB and IVA with curative intent were used for the studies and those with para-aortic

metastatic nodes (stage IVB) to the level of L2 vertebrae were also eligible. It excluded patients with further metastasis. All patients included received both EBRT and BT and the summation of doses calculated using a biologically equivalent dose in 2 Gy per fraction. The elective target for nodal disease was treated with 45-50 Gy by using EBRT only. It was reported by (Taylor et al., 2005), that metastatic pelvic and para-aortic nodes should be treated with combined interstitial-intracavitary brachytherapy or by a simultaneous integrated EBRT boost to a of 55-65 Gy.

Per the recommendations of the study, physical examinations, blood tests, gynecological examination, biopsy of primary tumor, imaging of pelvis by MRI, imaging of thorax by MRI, imaging of retroperitoneal space and abdomen and staging according to FIGO and TNM must be done before treatment commences and no investigation should be more than 4 weeks old at the time of treatment initiation (Nomden et al., 2019).

Treatment planning for EBRT is performed using a 3D dose planning system which is based on a 3D CT data set, with slice thickness not more than 3-5mm. In prone position, the belly board may be used in certain situations and supine position should be used if para-aortic irradiation is planned (Adli et al., 2003).

In 2016, GEC-ESTRO GYN network launched EMBRACE II which is a prospective interventional study with specific treatment interventions based on recommendations of EMBRACE I. The study aimed to benchmark the excellent outcome which was overall survival, local, modal and systematic control, reduced morbidity and improved quality of life that can be achieved by optimal delivery of advanced EBRT and brachytherapy techniques. It also aimed to implement systematic contouring, prescription and reporting for EBRT CTV and OARs (Petric et al., 2009).

EBRT must be delivered as IMRT/VMAT with cone beam CT (IGRT) in 25 fractions with 1.8 Gy to a total dose of 45 Gy given in 5 weeks. Target definition is MRI based (initial GTV) for the CTV-T with an initial high risk (HR) and low risk (LR) CTV-T and an ITV-T. MRI based nodal target (CTV-Elective) is according to risk of nodal spread, small pelvis, large pelvis or large pelvis + para-aortic region. Overall CTV/ITV to PTV margin is 5 mm. Involved lymph nodes are boosted with 10-15 Gy and treated as simultaneous integrated boost (SIB) within 5 weeks (2.2 - 2.4 Gy per fraction). The CTV-T and the CTV-E must be treated to 45 Gy using EBRT (PTV 45). Risk allocation is based on primary tumor characteristics and nodal pathology during diagnosis and considers the probability of developing lymph node metastasis in pelvic and para-aortic areas. Doses to the PTV45 should be homogeneous with at least 95% covered by the 95% prescription isodose and dose maximum less than 107% of the prescribed dose (Lutgens et al., 2003). Attention is needed for the organs at risk near the CTV-T HR (bladder, rectum, sigmoid and bowel).

The recommendation given within this protocol for the nodal boost is that total EBRT + BT dose should be in the range of 55-60 Gy EQD2. The total dose to PTV-Ns of about 60 Gy EQD2 can be achieved with the following fractionation schedules; inside true pelvis, EBRT with simultaneous integrated dose (SIB) 25x2.2 Gy =55 Gy physical dose. This is equivalent to 56 Gy EQD2 EBRT + 3-4 Gy EDQ2 from brachytherapy which results in a total dose of approximately 60 Gy EDQ2 (Groenen et al., 2018). Outside the true pelvis, EBRT with SIB 25x2.3Gy =57.5Gy physical dose. This schedule is equivalent to 59 Gy EDQ2 and brachytherapy dose contribution is negligible.

2.6 QUALITY ASSURANCE

Quality assurance in radiotherapy refers to all procedures that ensure consistency of the medical prescription and safe fulfillment of that prescription, as regards the dose to the target volume, together with minimal dose to normal tissue, minimal exposure of personnel and adequate patient monitoring aimed at determining the end result of the treatment (Williams et al., 2000). The growth in complexity of the entire radiotherapy process suggests an increased probability of errors and requires the development of improved mechanisms to ensure optimal treatment quality. Record and verify systems have been used for monitoring treatment parameters and although such systems reduce random errors in the delivery process, transfer and application of treatment parameters can increase the amount of systematic errors in treatment delivery (Esch et al., 2000). Intensity modulated radiation therapy and volumetric modulated arc therapy MRT have become standard practice in radiotherapy and the dose delivered needs to be verified against the calculated dose distribution by the treatment planning system (Alber et al., 2008).

Regular patient-specific quality assurance can be regarded as overall system check where multiple parameters are varied simultaneously and provides a general impression of the machine performance. This governs all procedures which influences the consistency or accuracy of the radiation prescription either to the target volumes or the surrounding normal tissues (Podgoršak, 2005). A QA program is necessary to identify ambiguities and to check treatment compliance. It should also include a feedback procedure in all steps of radiation treatment (prescribed dose, treatment planning, patient positioning). Local audits are also an essential part of every QA procedure. Corrections should be communicated and implemented immediately after an error is tracked (Fowble et al., 2000).

At the end of commissioning measurements, before the radiotherapy equipment is put into clinical use, quality control tests should be established, and a formal quality control program initiated that will continue for the clinical lifetime of the equipment. After any significant repair, intervention or adjustment or when there is any indication of a change in performance as observed during planned preventive maintenance or routine quality control programs, additional quality control tests should be performed (Hurkamns et al., 2001). Appropriate measuring equipment should be used for any quality control test. All such equipment should be subject to an appropriate maintenance and quality control program. Tolerances set for the parameter must consider the uncertainty of the measurement technique. If a measurement is within tolerance, no action is required but if it exceeds the action level, immediate action is necessary, and the machine must not be used clinically until the problem is corrected and the correction is verified by measurement. All planning data should be independently checked including the plan integrity, MU calculations, irradiation parameters. All data entered as the interface between the planning process and the treatment delivery process should also be checked. Dose or dose rates in radiotherapy can be measured using dosimeters which are used in acceptance tests and regular performance tests of radiotherapy units and are an essential tool in a QA program. Ionization chambers are generally used to determine the absorbed dose in water at several photon and electron beam qualities but are calibrated in air.

2.7 SCANDIDOS DELTA4 PHANTOM

Commercial systems such as ArcCheck, Octavius and Delta4 phantoms are being used for VMAT QA. The ArcCheck system contains 1386 n-Si diodes placed on a cylindrical surface of 21 cm diameter inside a ring-shaped PMMA phantom. These detectors, 1cm apart, form 21 helical continuous rings with 66 detectors on each ring. The system acquires data at every 50ms during treatment delivery which are converted and accumulated to composite dose for subsequent analysis. The Octavius-4D is composed of a polystyrene cylindrical phantom, rotating together with the gantry, coupled with a 729 ionization chamber array (Wolfsberger et al., 2010).

The Delta4 system consists of 1069 p-type silicon diodes in a crossed array inside a cylindrical polymethylmethacrylate (PMMA) phantom and associated software allows the user to compare the measured dose distribution for a complete treatment plan with the dose distribution predicted by the TPS. The diodes are cylindrical, have an area of 0.0078 cm^2 and are spaced 0.5 cm intervals over the central 6 x 6 cm of the planes and at 1cm intervals over the remainder of the central 20 x 20 cm of the planes. The crossed planes are achieved by means of a main detector board which passes through the entire diameter of the phantom and two wing detector boards which are separated to allow the main detector board to pass between them. The phantom itself has a diameter of 22 cm and length of 40 cm.

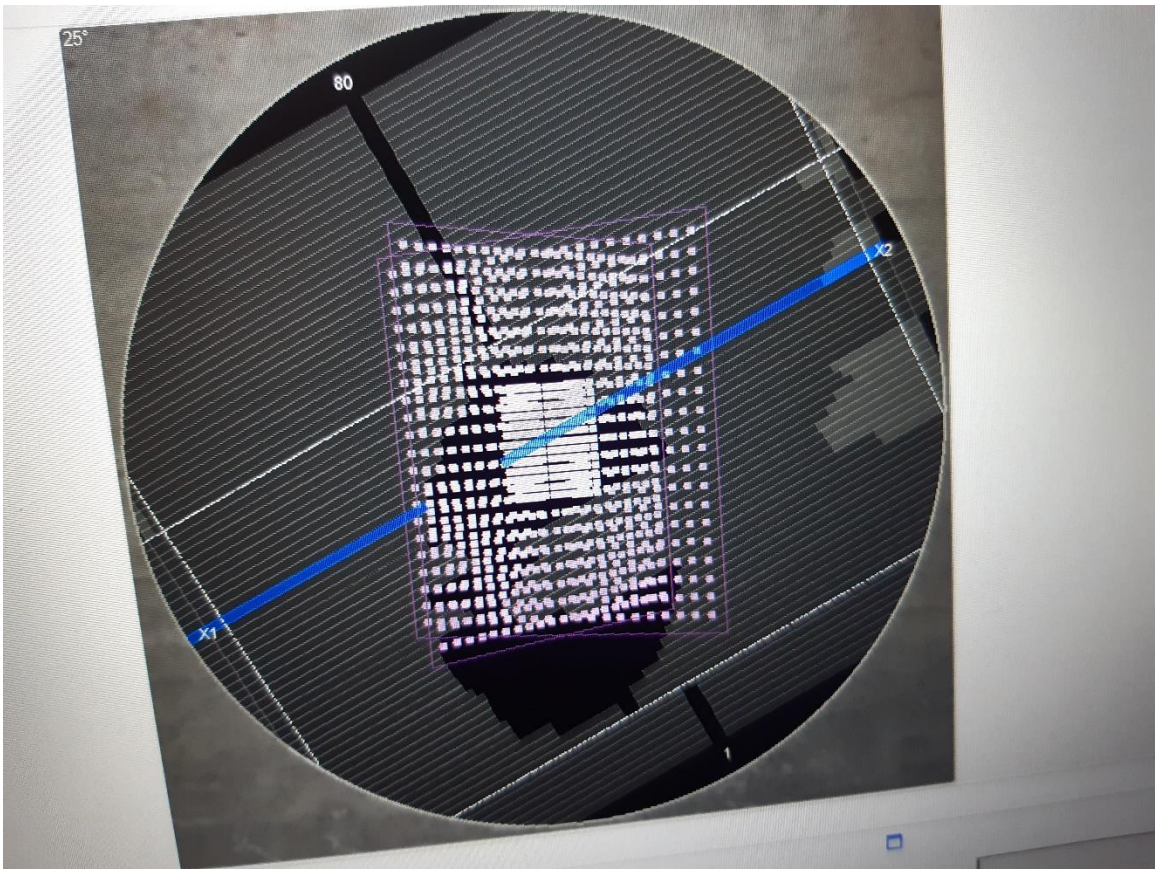

Figure 2.4: A cross-sectional view of the Scandidos Delta4 phantom showing the numerous detectors.

The device records the measured dose in relation to the individual accelerator pulses by using a trigger signal from the accelerator thereby facilitating time-dependent four-dimensional applications (Baldock et al., 2010). Gantry angles are in some instances independently sensed by means of an inclinometer attached to the gantry or accelerator head. This allows the device to identify which control point of a dynamic arc delivery is being delivered so that the measured dose can be associated with this control point and the appropriate correction for gantry angle applied. Delta4 uses the planned 3D dose distribution to calculate the gamma index. The planned dose grid used for calculation of the gamma-index is interpolated from the original planned dose grid. This interpolation is

necessary since only few detectors happen to be in the same position as nods of the planned dose grid. The spatial resolution of the interpolated dose grid is the same as the original resolution (Morele et al., 2015).

In a study to determine the ability of Delta4, Octavius and Compass systems in detecting simulated machine output and MLC calibration errors in VMAT delivery, it was reported by (Alvarez and Fabian, 2010) that Delta4 system detected 15 out of 20 simulated errors whilst the Compass and Octavius detected 8 out of 20 errors. Delta4 is more sensitive to MLC position (M. Hussein et al., 2013).

2.8 GAMMA INDEX

The 3D gamma index is one of the metrics which have been widely used for routine patient specific quality assurance for IMRT, tomotherapy and V0MAT. This compares the calculated plan dose distribution to the measured dose distribution. Depending on the normalization value of the dose difference between measured and calculated dose points, there are two methods for calculating the gamma index which are local calculation method and the global calculation method (Negri et al., 2014). With the local normalized method, the TPS calculated dose corresponding to the point measured is used to determine the acceptable dose difference criteria when determining percentage error. In the global calculation method, the acceptable dose difference criteria use the maximum dose found in the patient plan dose. The global gamma-index is seen by majority of physicists as the standard method. The γ gamma) technique compares dose differences at specific points and determines the distance to the nearest point which have the same dose value. The dose

difference criterion is important in low dose gradient regions while the distance-to-agreement criterion yields valuable information in regions having a high dose gradient. The dose difference and distance-to-agreement criteria can be selected and often values of 3 %/3mm are used (Low, 2003). The criteria of 3% 3mm were used due to the limitations of TPS algorithms where penumbra modelling was a source of uncertainty .

Points lying inside the ellipse with axes having the criteria values have a gamma value equal or smaller than one. Since the dose difference is a percent value, the local gamma index analysis could exaggerate the dose difference in the low-dose regions and the global gamma index method could also underestimate the dose discrepancies in the low-dose regions (Stathakis et al., 2014).

It was proposed by (Hielemann et al., 2013), that a stricter gamma index (2% 2mm) is necessary to detect positional errors of the MLC. However, the quality assurance procedure of VMAT treatment plans must involve detailed examination of where dose deviations occur and professional judgement is needed when interpreting the gamma-index analysis since even a greater than 90% passing rate using 2% 2mm gamma-index criterion does not guarantee the absence of clinically significant dose deviation. The configuration and resolution of the detector have a great impact on the calculation of the gamma passing rates. It was reported by (Hussein et al., 2013) that the gamma passing rates of VMAT depend on the type of dosimeter used. To make use of the gamma index analysis for the verification of the VMAT delivery accuracy, it is necessary that each institution establishes their own gamma analysis protocol by determining the type of the gamma index analysis and gamma criterion with their own linac and dosimeter. The gamma-index provides an efficient

analysis and has been used effectively within dosimetry audits of complex radiotherapy plans (Lievens et al., 2009).

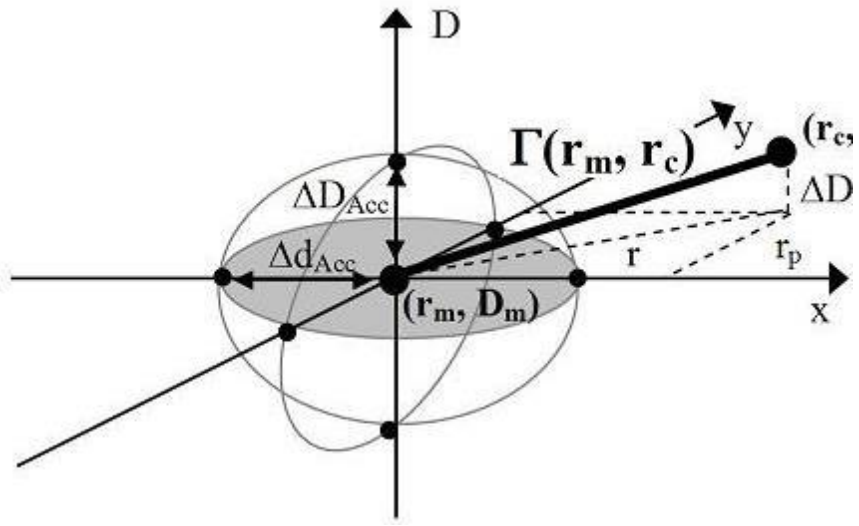

Figure 2.5: Gamma analysis for a 2D dose distribution (Xing et al., 2015).

D_c: calculated dose (i.e. planned dose) in position r_c

D_m: Measured dose in position r_m

$r = r_m - r_c$

$\Delta D = D_m - D_c$

ΔD_{Acc}: Acceptable dose difference

Δd_{Acc}: Acceptable spatial deviation

$$\Gamma(r_m, r_c) = \sqrt{\frac{r^2(r_m, r_c)}{\Delta d^2_{Acc}} + \frac{\Delta D^2(r_m, r_c)}{\Delta D^2_{Acc}}} \quad \text{equation 1}$$

During gamma-index calculation, it is checked if the calculated dose distribution surface intersects with the ellipsoid representing the acceptance criteria. The calculation passes if the gamma index is smaller or equal to 1, otherwise it fails. The distance to agreement

method (DTA) compares two dose distributions. For each measurement point, the distances to all those points in the calculated dose distribution that have the same dose as the measurement point are calculated. The shortest distance for each point is the DTA. Gamma index is not sufficient and attention must be paid to the discrepancies between calculated and measured dose (Sharfo et al., 2015).

There is variation between gamma pass rates between commercially available gamma analysis software. The gamma index calculated by Octavius 4D dosimeter system and 3DVH were compared with manually calculated for one data set. The gamma pass rate calculated by these systems was compared using 3% 3mm, 2% 2mm and 2% 3mm. The gamma indexes calculated by the two systems were accurate but gamma pass rates were different due to the different interpolation of raw dose data by the two systems and different implementation of gamma index calculation and other modules (Xing et al., 2015).

2.9 FLATENNING FILTER AND FILTER FREE RADIATION

Linacs can deliver filtered beams (FB) and flattening filter free (FFFB) photon beams. The use of flattening filter free beams have boosted treatment delivery as the removal of a flattening filter causes more efficient photon production and increased dose rate substantially at treatment level. To improve dose delivery efficiency, the dose rate can be increased by removal of the flattening filter and the resulting flattening filter free (FFF) beams have a cone-shaped dose profile and up to a fourfold higher dose rate in the center of the beam with respect to the flattened beams (Kragl et al., 2009).

Increased dose rate results in shorter treatment time and reduces intrafraction motion which enhances patient's treatment comfort (Kumar et al., 2017). FFFB offers other dosimetric advantages such as reduced scatter, reduced leakage and reduced out of field scatter doses (Georg et al., 2011). This reduction in out of field doses may lead to minimizing the risk of radiation induced secondary malignancies. It was reported by (Ramtohul et al., 2011) that the use of FFFB reduces scatter and associated dose to distal organs, means FFFB is associated with a lower secondary dose to distal normal organs than FB of the same photon energy. According to (Park et al., 2013), there were significant increment in target mean dose for FFFB as compared to FB for both 6MV and 10MV photon beams. Also, FFFB was found to deliver slightly higher mean target dose compared to flattened beams. For organs at risk like the bladder and rectum, flattening filter free beams delivered slightly higher mean dose and dose volumes in comparison to flattened beams of 6 and 10 MV for prostate cancer. According to (Chieregato et al., 2018) the FFF technique delivers an equal or better dose distribution with a major reduction of treatment time and number of apnoeas.

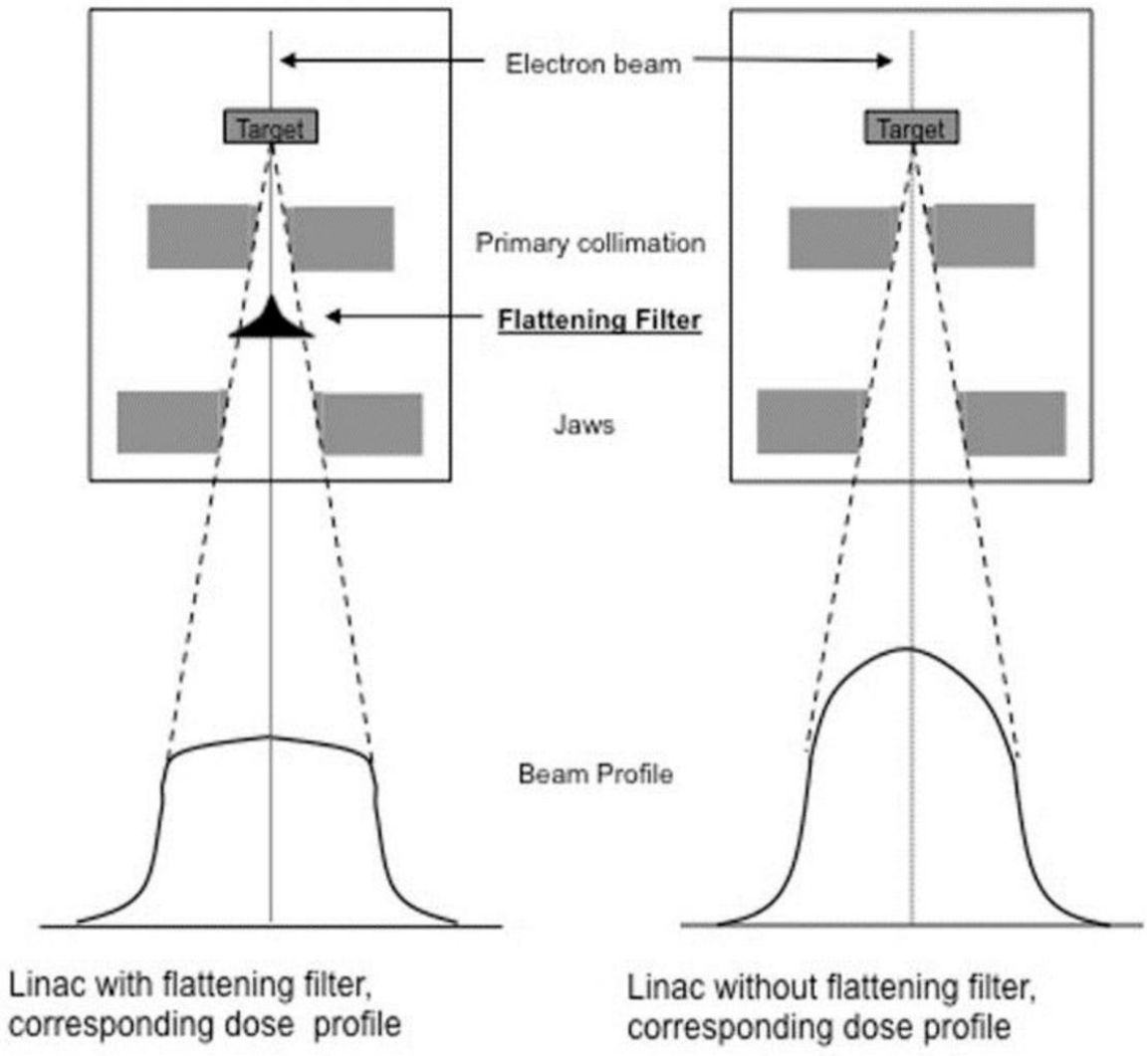

Figure 2.6: A linac with and without the flattening filter showing fluence profiles of photon beams (Balik et al., 2018).

It was concluded that increased mean target dose indicated that homogeneity in target become worse and also FFFB generates inferior homogeneous dose distribution compared to FB (Lalit et al., 2017). Flattening filtered beams also spare more bladder and rectum when compared to FFFB in cervical cancer treatment and this reduces the toxicity level to the patients (Suresh et al., 2018). FB also generates more conformal and homogeneous

plans compared to FFB. It was reported that FB is more beneficial for cervix treatment than FFFB (Titt et al., 2006).

For sinonasal cancer treatment, FFFB generated comparable target dose conformity, homogeneity, reduced normal-tissue doses and increased number of MUs compared with flattened beams in both IMRT and VMAT. The FFFB exhibited improvements in contralateral optic structures and other critical structures and provided comparable overall OAR sparing and delivery efficiency in VMAT (Lu et al., 2016). The clinical application of FFF beams have been studied for breast cancer, lung cancer and other tumor sites and it was concluded that the FFF beams produced similar plan qualities and reduction of treatment time. It was reported by (Kragl et al., 2009) that large field VMAT with flattening filter free beams using half beam blocks can produce highly homogenous dose distributions to multiple target volumes and generates high dose gradients to spare nearby critical structures better than conventional VMAT techniques .

2.10 MULTILEAF COLLIMATOR

MLCs provide a solution to the problem of molding, use and storage of blocks. It provides conformal fields by using more treatment angles without having to deal with large number of blocks. The Elekta MLC consists of 40 pairs of tungsten alloy leaves with 7.5 cm thickness and each projecting a 1.0 cm leaf width and 32.5 cm leaf length at the isocenter (Boutevin et al., 2013). Tungsten alloys are hard, simple to fashion, and have a low coefficient of thermal expansion. The distance a leaf can travel over the center of the field is 12.5 cm and the maximum leaf speed is 2.0 cm/sec at the isocenter. The use of MLC

field shaping saves time and incurs a lower operating cost when compared to the use of beam blocks.

To decrease radiation leakage through the very small gap between any 2 leaves, the side of each MLC leaf is designed so that one side of the leaf has an extended portion called the tongue and the side of the adjacent leaf has an indented portion called the groove. The two adjacent leaves are coupled together through the tongue and the groove to lessen the leakage radiation. The Elekta MLC have additional backup jaws that travel in the same directions as the MLC and are full in the sense that they are not segmented. When adjacent leaves have different degrees of extension, the tongue side of the more extended leaf produces a underdose region near the leaf edge (McNiven et al., 2004). The collimator is rotated to minimize interleaf leakage and tongue-and-groove effect.

Ideal choice of collimator angle can increase the optimization degree freedom to shape a desired dose distribution. At a zero angle, the sum of leakage MLC accumulated during gantry rotation can result in unwanted dose distribution, which cannot be controlled by optimization. When the collimator angle increases up to 45 degrees, the penumbra and irradiation volume will spread due to field size of the inferior to superior axis jaw being larger than the collimator angle at zero degree. The characteristics of VMAT technique is the use of dynamic multileaf collimators which enable leaf motion during treatment delivery. Leaf shape and width helps to achieve the dose distribution. Delivered dose can directly be affected by errors in MLC positioning (Orlandini et al., 2015).

Typical MLCs have 40 to 120 leaves arranged in pairs. By using the computer controls to position many narrow, closely abutting leaves, an arbitrarily shaped field can be generated. By setting the leaves to a fixed shape, the fields can be shaped to conform to the tumor.

Leaf acceleration and deceleration have a negligible effect on the delivered intensity profiles but a sluggish leaf can affect the gap width during delivery and the MLC software can modulate the dose rate by adding beam holdoffs (Essers et al., 2001).

2.11 MONITOR UNITS (MU)

A monitor unit is a measure of machine output from a clinical accelerator for radiation therapy such as a linear accelerator or an orthovoltage unit. Monitor units are measured by ionization chambers that measure the dose delivered by a beam and are built into the treatment head of linear accelerators (Halperin et al., 2008). The output from a linac is measured as charges in the ionization chamber. The ionization chamber read out 100 MU when an absorbed dose of 1 Gy is delivered so that the specified point is at the isocenter of the machine and the field size is 10 x 10 cm at a depth of 10 cm in water.

The monitor units needed to deliver a treatment plan are calculated by the treatment planning system. Dose errors arising in computing the MU could potentially affect the whole course of treatment. MU is affected by beam energy, source surface distance (SSD), tissue-phantom ratio/tissue maximum ratio, percentage depth dose (PDD), output factor (OF), wedge factor (WF) and calibration factor (CF) (Huang et al., 2015). Increasing SSD will mean that MU will be required to deliver a dose at depth due to the effects of the inverse square law and this must be taken into account and is usually only a problem for extended SSD treatments (Jimenez-Puertas et al., 2018).

2.12 TREATMENT PLANNING

It is the process by which radiotherapy device is programmed to deliver an amount of radiation to a patient (Baumer et al., 2017). The treatment planning process involves many steps and the medical physicist is responsible for the integrity of the computerized TPS to accurately and reliably produce dose distributions and associated calculations for EBRT. This includes acquisition of beam data, treatment plan generation and the transfer of data to the treatment machine. CT based computerized treatment planning provides the ability to view dose distributions directly superimposed upon a patient's axial anatomy.

The quality of the treatment is closely linked to the accuracy of dose calculation performed in the TPS where all the simulation can be done and evaluated (Dursun et al., 2016). TPS is the heart of the radiotherapy process. Once image datasets are loaded, a contouring step identifies the volumes of interest (clinical target volumes, gross tumor volume) then the system develops a complex plan for each beam line route for how the therapy system will deliver the radiation to the target volume. It calculates the expected dose distribution by recognizing the dose tolerance for each organ inside the concerned patient by using the required algorithms. The algorithms used can be classified into the correction-based algorithm and the model-based algorithms.

The correction-based algorithm makes several measurements of dose distribution in water phantom and corrects the expected dose values by taking some parameters into consideration such as depth, dimension of the boundaries and the path lengths. In the Model Based Algorithm, several parameters must be accounted to make an accurate distribution of dose and some of these are the size of the source, angular distribution of photons and

primary transmission, the electron contamination and tissue heterogeneities. The model-based algorithms perform the dose calculation directly in a patient representation. The dose calculation algorithms with their different principles is to provide a good description of the physical processes for primary and secondary particles by simulating their transport inside the medium where dose distribution optimization is performed and then simulate the deposition of the energy in the different tissues (Moore, 2019). Superposition and convolution algorithms used to calculate the dose distribution yielded almost the same results when the medium was homogeneous or less dense, and difference in the dose distribution is observed if the medium is non-homogeneous (Muhammad et al., 2011).

Monte Carlo techniques generate dose distributions by following the histories of a large number of particles as they arise from the radiation source and undergo multiple scattering interactions both inside and outside the patient (Reynaert et al., 2007). It precisely models the physics of particle interactions and accounts for the geometry of individual linacs, beam shaping devices (blocks and MLCs) and patient surface and density irregularities. This allows a wide range of complex patient treatment conditions. To attain a statistically accepted result, Monte Carlo techniques require the simulation of a large number of particle histories and this reduces the calculation time to an acceptable level.

Monte Carlo algorithm and Pencil beam algorithms are commonly used for electron beam dose calculations. The energy spread or dose kernel at a point is summed along a line in a phantom to obtain a pencil type beam or dose distribution. Integrating the pencil beam over the patient's surface to account for changes in primary intensity, and by modifying the shape of the pencil beam with depth and tissue density, generates a dose distribution (Machichi et al., 2019).

2.12.1 INVERSE PLANNING

It is a method of radiation treatment planning where one starts with the desired dose distribution or clinical objectives and then determines the treatment parameters that will achieve it. This is opposed to the conventional forward planning approach where the treatment parameters are first chosen and then the resulting dose distribution is calculated and evaluated. Since inverse planning begins with the description of the desired dose distribution, it represents a change of paradigm in the planning process. In inverse planning, the anatomical features and dose constraints constitute the starting point of the dose optimization process. The benefit of the inverse planning approach is that all clinical requirements such as dose coverage and normal tissue protection are simultaneously and automatically taken into account (Akartunalı et al., 2015). Conventional forward planning depends on geometric relationship between the tumor and nearby sensitive structures. Inverse planning is less dependent on the geometric parameters but more on specification of volumes of tumor targets and sensitive structures (Poon et al., 2007).

2.13 HOMOGENEITY AND CONFORMITY INDICES

Dose distributions can be estimated using dose-volume histograms (DVHs) and isodose lines but the large volume of data contained in these histograms are difficult to interpret. It is vital to find fast and simple tools that analyze dose distribution of treatment plans and help to choose optimum plans which provides maximum homogeneous tumor coverage and protects critical organs (Kataria et al., 2012). These tools comprise conformity index (CI) and homogeneity index (HI).

Homogeneity index (HI) is a fast and simple scoring tool that analyses and quantifies dose homogeneity in the target volume. It is used to evaluate, compare the dose distributions of various treatment plans and choose the best plan among available plans. It also serves as a guide for development of future technology and treatment protocols as it can compare various devices or techniques (Cirino et al., 2012). HI indicates the ratio between the maximum and minimum dose in the target volume and a lower value indicates better homogenous dose distributions. HI can be defined in several ways and a common definition is; HI = $D_{5\%}$ / $D_{95\%}$ where $D_{5\%}$ and $D_{95\%}$ are minimum dose to 5 and 95% of the target volume respectively. The ideal value of HI is 1 and it implies a perfect homogeneity of the dose distribution and it increases as the plan becomes less homogeneous. An increased homogeneity index implies poorer homogeneity (Collins et al., 2006).

The conformity index (CI) measures how well the distribution of dose matches with the target volume. It is defined by the Radiation Therapy Oncology Group (RTOG) as a ratio between the volume covered by the reference isodose (RV) which according to ICRU is the isodose of 95% and the target volume designated as PTV. It is given by the equation

$CI_{RTOG} = V_{RI} / TV$ (Sasaoka et al., 2011). A conformity index of 1 represents the ideal dose coverage or high conformity. A conformity index greater than one implies that irradiated volume exceeds the target volume and covers part of the healthy tissue. If the CI is less than one, the target volume is partially irradiated.

RTOG criteria define a range of CI values to determine the quality of conformity since the value up to 1 can hardly be reached. If the conformity index is between 1 and 2, the treatment agrees with the protocol; between 2-2.5 and 0.9 – 1, it is considered that there is

a minor deviation from the protocol. If it is greater than 2.5 and less than 0.9, it implies a severe deviation from the protocol (Georges et al., 2006).

CHAPTER 3

3 METHODOLOGY

3.1 INTRODUCTION

This chapter describes the methodology and materials used to obtain the results for this research. It consists of the study site, study population, sampling procedure, inclusion and exclusion criteria, data collection and data analysis tool.

3.2 STUDY SITE

The study was conducted at the Radiotherapy Department of the St. Olavs Hospital in Trondheim, Norway. St. Olavs Hospital is the university hospital for Mid-Norway and integrated with the Norwegian University of Science and Technology (NTNU). Patient treatment, research and education of health professionals are integrated functions. The department currently has 5 Elekta linear accelerators, a CT simulator and a high dose rate brachytherapy machine.

3.3 STUDY POPULATION

The selected population for this study were patients who were included in the EMBRACE I study. These patients received conventional treatment during the EMBRACE I study. Based on the recommendations of the EMBRACE I, EMBRACE II was developed which

served as a golden standard for cervical cancer treatment. The EMBRACE II study was a prospective interventional study involving 26 different centers to systematically apply IMRT/VMAT with daily image guided radiotherapy as well as advanced adaptive brachytherapy (IGABT), implement a dose prescription protocol for (IGABT), implement systematic contouring, prescription and reporting for external beam radiotherapy CTV and OARs (Tan et al., 2018). In all, 1416 patients with cervical cancer were used for the entire EMBRACE I study. Out of this number, 37 patients were included in the EMBRACE study at the St. Olavs Hospital.

Using the golden standard based on the findings from EMBRACE II, the EBRT plans of these patients were recalculated hence the treatment plans used in this study had not been given to the patients.

3.4 SAMPLE SIZE

For this study, only patients with pathological pelvic lymph node metastasis were included. 15 patients out of the 37 patients with cervical cancer who took part in the EMBRACE I study had pelvic lymph node metastasis. The patients had already received conventional radiation treatment as part of the EMBRACE I study. It was convenient to use data from these 15 patients with pelvic lymph node disease because they had already signed consent for their plans to be used for studies. The 15 patients used for this study had different numbers of positive lymph nodes. Based on CT images, the locations of these positive lymph nodes differed from patient to patient.

3.5 SAMPLING

Samples were selected using total enumeration sampling. This is also known as consecutive sampling. With this technique, every subject which meets the inclusion criteria is selected until the required sample size is achieved (Bowers et al., 2011). Also, this is a non-probability sampling technique where samples are picked at the ease of the researcher which is more like convenience sampling but with a slight variation. Consecutive sampling is relatively easy to employ. Researchers choose to use this method because the size of the population that has the particular set of characteristics that is of interest is very small. Total enumeration sampling technique can be considered as the best of all non-random samples since it includes all subjects that are available and makes the sample a better representation of the entire population (Rothman et al., 2008).

3.5.1 EQUIPMENT

The equipment used included three Elekta linear accelerators, ScandiDosdelta4 phantom (Uppsala, Sweden), Raystation treatment planning system from Raysearch Laboratories AB, Sweden (6R, v5.99.0.5) and a thermometer.

3.5.1.1 ELEKTA LINEAR ACCELERATOR

The radiotherapy department currently has 5 linear accelerators but three of these were used for the study and are named SB3, SB5 and SB6. The SB3 Elekta linac has the longest operational time followed by SB5 and SB6 which was the latest to be installed. SB refers to the Norwegian abbreviation for radiation treatment. All three linacs produce both photon

and electron beams of various energies. They have multileaf collimators (MLC) to provide conformal shaping of photon treatment beams and have the ability to carry out IMRT/VMAT treatment. The photon beam energies ranges from 6 MV – 15 MV.

All the linacs used for this study have an on-board cone beam CT. The cone beam imaging is an advanced computed tomography technology unit that is part of the linear accelerator and helps to see a 3D image of patient's anatomy and the area that is being targeted immediately before the radiation treatment is delivered. This imaging takes about a minute and it is non-invasive. It also reduces the chances of treatment side effects.

Figure 3.1: An image of one of the linear accelerators (SB6) used in the Radiotherapy department of the St. Olavs Hospital.

3.5.1.2 SCANDIDOS DELTA4 PHANTOM

The Delta4 phantom has two crossing arrays in a fixed cylindrical geometry and provides full coverage of the cross-section of any beam direction. It is the 3D solution that verifies the dose gradients in X,Y and Z directions by real measurement in the target. The design with two crossing arrays optimizes the use of a fixed number of detectors in radiation therapy. Each detector independently measures dose, pulse, pixel and builds the 4D dose-picture. This benefits the user by enabling full flexibility in adaptation to any possible dynamic treatment. With Delta4, the cause of a discrepancy can be traced and analyzed (Capomolla et al., 2018).

Delta4 measures the dose with high density in the high gradient region with a resolution of 50 nGy (Fontaine et al., 2018). It has 1069 detectors which are built in two orthogonal planes with a resolution of 0.5 cm in the center and 1cm at the periphery. Each diode is a cylinder of 0.5 mm diameter and height of 0.05 mm.

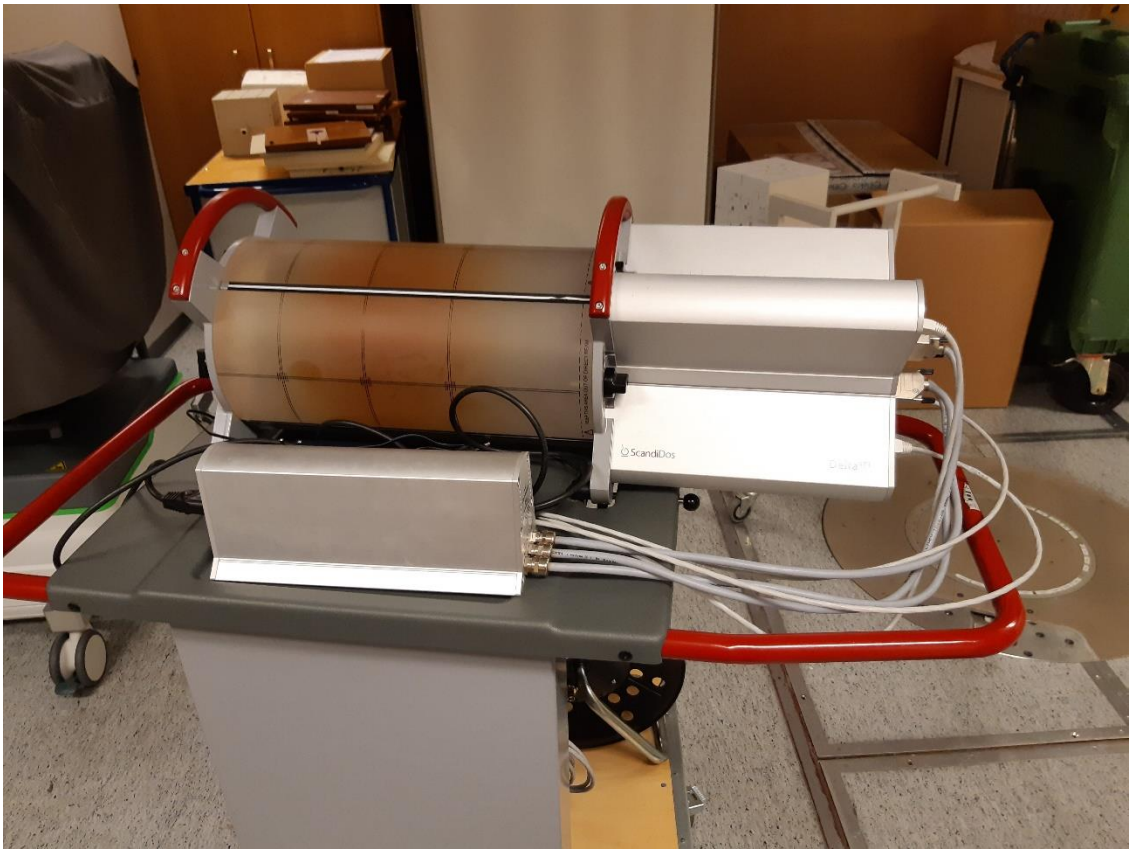

Figure 3.2: An image of the Delat4 phantom (from ScandiDos AB, Sweden) used in the radiotherapy department.

3.6 DATA COLLECTION

To ensure there is no breach in confidentiality, the names of the 15 patients/plans were removed and replaced with pseudo names. Treatment plans were named; PT1, PT2, PT3, PT4, PT5, PT6, PY7, PT8, PT9, PT10, PT11, PT12, PT13, PT14 and PT15 respectively. All treatment plans for both the 6MV and FFF beams met the dose constraint requirements for the primary tumor as well as the lymph node volumes.

The Delta4 phantom was transferred from the phantom trolley to the treatment couch. It was aligned on the couch using the set-up lasers at the phantom's isocenter. It was then connected to the linac using cables and then to the computer containing the ScandiDos Delta4 software (version 2014).

Figure 3.3 An image of the setup of the Delta4 phantom on the linac for measurement.

The room temperature was measured to be 23.6 degrees Celsius (°C). Measurements were done using both conventional 6 MV beam with flattening filter and flattening filter free beam (FFF) for all 30 VMAT plans. Each patient thus had a 6 MV plan and an FFF plan.

The first set of measurements were done using the SB3 linear accelerator. The factor of the day which is a calibration correction factor was first determined for both 6 MV beam

and the FFF beam. This means that all measurements using the conventional 6 MV flattening filter would be corrected for using this factor and same for the FFF beams. The factor of the day was determined by aligning the lasers at the isocenter of the phantom to ensure correct geometrical positioning and radiating the phantom with a dose of 1 Gy (MU=108), field size of 10 x 10 cm and at a gantry angle of 270 °C. After this, the gantry was rotated to 90 °C and the phantom was radiated using the same treatment parameters. The ScandiDos software gave the factor of the day. The same procedure was repeated using the FFF mode and the factor of the day was recorded.

The treatment plans were made using two arcs and then delivered to the delta4 phantom; arc 1 (178°- 182°) and arc 2 (182° - 178°) for the 6MV beams and arc 3 (178°- 182°) and arc 4 (182° - 178°) for the FFF beams. Treatment plan PT1 was the first plan delivered using the 6 MV beam followed by the FFF beam to determine the gamma pass rate, dose deviation, distance to agreement and the median. The procedure was repeated for the rest of the treatment plans. All measurements using the SB3 was done in one day.

Figure 3.4: An image showing the setup for determining the factor of the day for both 6 MV and FFF beam at 90°.

The measurements for the SB3 was then repeated at a later date after linac optimization where there was tuning of the linear accelerator. The machine optimization was done by the service engineers. The measurements were repeated to determine if gamma pass rate and associated indicators would improve after machine optimization. This procedure involved adjusting the gun filament to get an optimal current for producing treatment beams. This was done using both photon and electron beams. If the startup current is too

high, more electrons would be produced at the filament and energy would be wasted. If the startup current is also too low, the beams would be produced at a slower rate. Since the filament burns out after long period of use, there's the need to optimize the gun filament. If the filament current falls far below the required current, then the gun filament must be changed. The new filament current determines the maximum dose rate of the linac.

Figure 3.5: An image showing the linac at 178° before VMAT treatment delivery.

The next set of measurements were done using the SB5 linear accelerator. The same procedure as done using the SB3 was replicated using the SB5. The room temperature recorded was 23.6 °C and the factor of the day for both the 6 MV and FFF beams were recorded. Also all the measurement using the SB5 were done on the same day. There was also machine optimization of the SB5 linear accelerator and hence the measurements were repeated for both the 6 MV and the FFF beams.

The last set of measurements were done using the SB6 linear accelerator. All 30 VMAT plans were delivered using the same procedure as that of the SB3. The factor of the day for the 6 MV was also determined.

3.7 DATA ANALYSIS

The data was analyzed using mathematical analytical tool MATLAB R2015a (The Math Works Inc., Natick, Massachusetts US.MATLAB R2015a, 2015). MATLAB allows matrix manipulations, plotting of functions and implementation of algorithms. Results were also plotted using MATLAB.

Wilcoxon signed rank test was used for statistical analysis of the data because of the small sample size. It is a non-parametric statistical hypothesis test used to compare two related samples, matched samples or repeated measurements on a single sample to assess whether their population mean ranks differ (White, 2017). It is appropriate for evaluating data from a repeated design in a situation where the prerequisites for a dependent samples t-test are not met.

The Wilcoxon signed-ranked test is used to test differences of paired data without the normal distribution assumption of the differences that is required for the paired t-test (Kerby, 2014). This signed rank test was done using MATLAB function signrank which returns the result of the hypothesis test performed at the 0.05 significance level. H = 0 indicates that the null hypothesis ('median is zero') cannot be rejected at the 5% level. When H =1, it indicates that the null hypothesis can be rejected at the 5% level. A p-value less than 0.05 was regarded as statistically significant. Trendlines were also calculated and plotted using the polyfit and the polyval functions.

CHAPTER FOUR

4 RESULTS AND DISCUSSION

4.1 INTRODUCTION

This chapter presents the results and discussion obtained from this study and includes gamma pass rates for conventional 6 MV beams and FFF beams, monitor units, volume of PTV and other parameters.

4.2 GAMMA PASS RATES

It is common to report the results of a gamma analysis as the percentage of points that achieved gamma index less than 1 which is the gamma passing rate. A gamma pass rate of at least 90% with 3%3mm was used as the clinical criteria for the pass rate. All plans with pass rate greater than or equal to the 90% pass rate were considered to have passed and those with pass rates lower than 90% were considered to have failed. This also means that if the gamma index is smaller or equal to unity, the calculation passes otherwise it fails. This is the criteria used by the Radiotherapy department of the St. Olavs Hospital. The 3%3mm criteria are based on the combined mechanical/dosimetric uncertainty contribution to the measured dose. Also the most commonest passing criteria used is the 3%3mm as proposed by (A. Low, 2003). This is also in line with (Mohamed et al., 2018) where it was proposed that the 3%3mm is the most appropriate of gamma criteria for quality assurance of VMAT plans.

4.2.1 GAMMA PASS RATES FOR 6 MV AND FFF BEFORE OPTIMIZATION (SB3)

The mean total gamma pass rate for the 6 MV was 91.9% with a standard deviation of 25.5 compared to the flattening filter free beam (FFF) which had a mean total pass rate of 89.5% and a standard deviation of 7.2. This implies that the 6 MV beam had a higher gamma pass rate than the FFF beam which had an average pass rate below the clinical criteria of at least 90%. The total gamma pass rate for the 6 MV beam was significantly higher than that of the corresponding FFF beam ($p = 0.0084$). This is in agreement with (Kumar et al., 2017) which concluded that filtered beams had a higher pass rate than FFF beams and hence more beneficial for cervix radiotherapy in comparison to FFF beams. This is also in line with (Bedford et al., 2009) where VMAT plan analysis showed higher values of 99% for all 6 MV beams and that of the FFF beams had the lowest value.

14 plans out of the 15 patient plans for 6 MV had gamma pass rate satisfying the pass rate criteria of at least 90%. However, patient plan PT12 could not be implemented because it was not technically feasible using the 6 MV plan on SB3 and the most probable reason could be that the treatment plan was too complex for the multileaf collimators on this linac. Also, the SB3 linear accelerator is the oldest amongst the three linacs used for this study and hence might not have been configured to execute certain complex plans. 7 out of the 15 FFF plans met the pass criteria with the lowest fail rate being 78.2%. The figure below indicates that the gamma pass rate is higher for the 6 MV plan than the FFF plan.

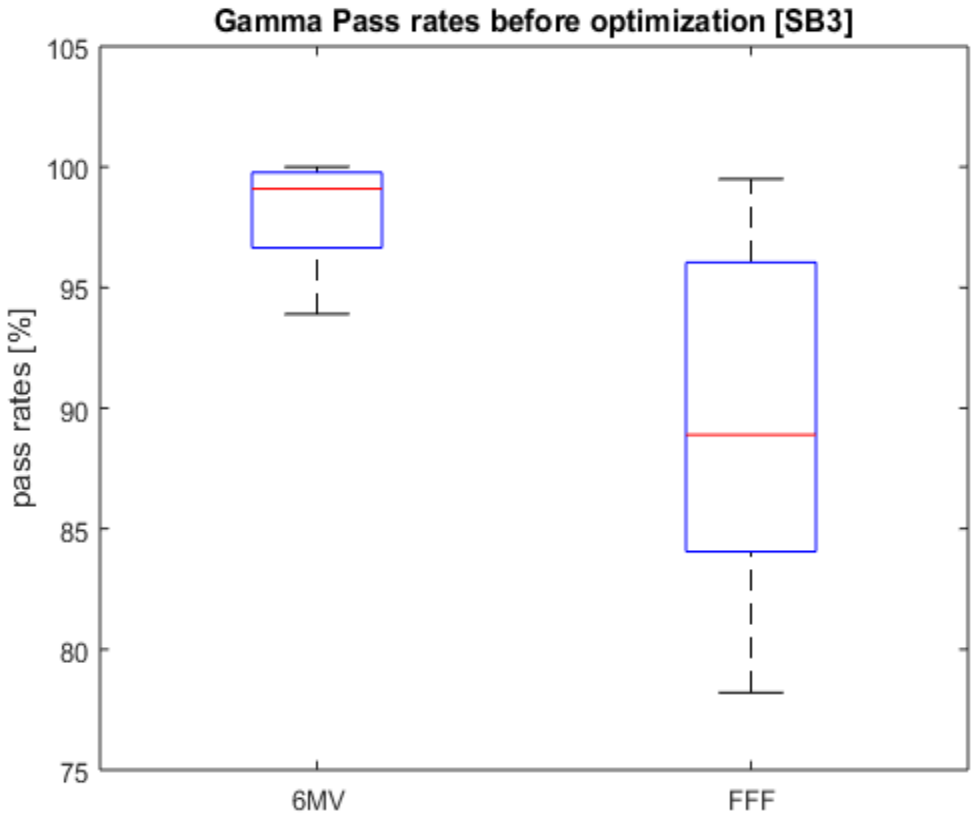

Figure 4.1: Boxplot of the gamma pass rate of 6MV and FFF before machine optimization of SB3. The upper and lower blue edges of the boxplot represent the 75th and 25th percentiles. The red line represents the median.

4.2.2 GAMMA PASS RATES FOR 6 MV AND FFF AFTER OPTIMIZATION (SB3)

After machine optimization, the mean total gamma pass rate for the 6 MV beam was 92.9% with a standard deviation of 25.7 and that of the FFF beam was 93.1% with a standard deviation of 4.9. This result was statistically significant with p = 0.0084. Also, after machine optimization, patient plan PT12 could not be implemented using 6 MV beam but was able to pass using the FFF beam. This affirms the fact that patient plan PT12 using the

6 MV is too complex for the SB3 linear accelerator. From figure 4.2 below, it can be observed that the gamma pass rate for the 6 MV was higher than that of the FFF beam.

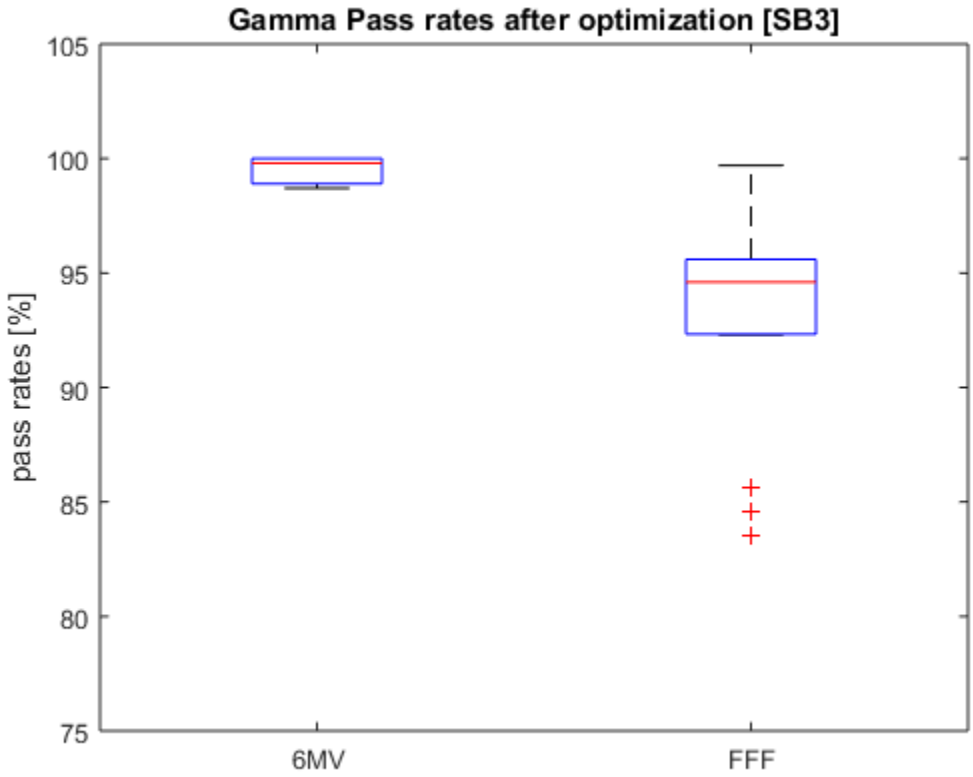

Figure 4.2: Boxplot of the gamma pass rate of 6 MV and FFF after machine optimization of SB5. The upper and lower blue edges of the boxplot represent the 75th and 25th percentiles. The red line represents the median. The red ‘’+’’ indicates possible outliers.

4.2.3 GAMMA PASS RATES FOR 6 MV AND FFF BEFORE OPTIMIZATION (SB5)

The mean total gamma pass rate for 6 MV was 98.7% with a standard deviation of 1.6 while that of the FFF was 91.7% and a standard deviation of 4.8. The total gamma pass

rate for 6 MV plans were significantly different from the total gamma pass rate of the FFF plans with p = 0.00006. All 15 6 MV plans had a gamma pass rate greater than the 90% pass criteria and two of these plans recorded a 100% pass rate. 5 out of the 15 FFF plans had a gamma pass rate below 90% indicating that these plans failed to pass. Figure 4.3 below indicates that the gamma pass rate for 6 MV is higher than the FFF plan and this implies that the 6 MV plans are more accurately delivered by a linear accelerator than the FFF plans.

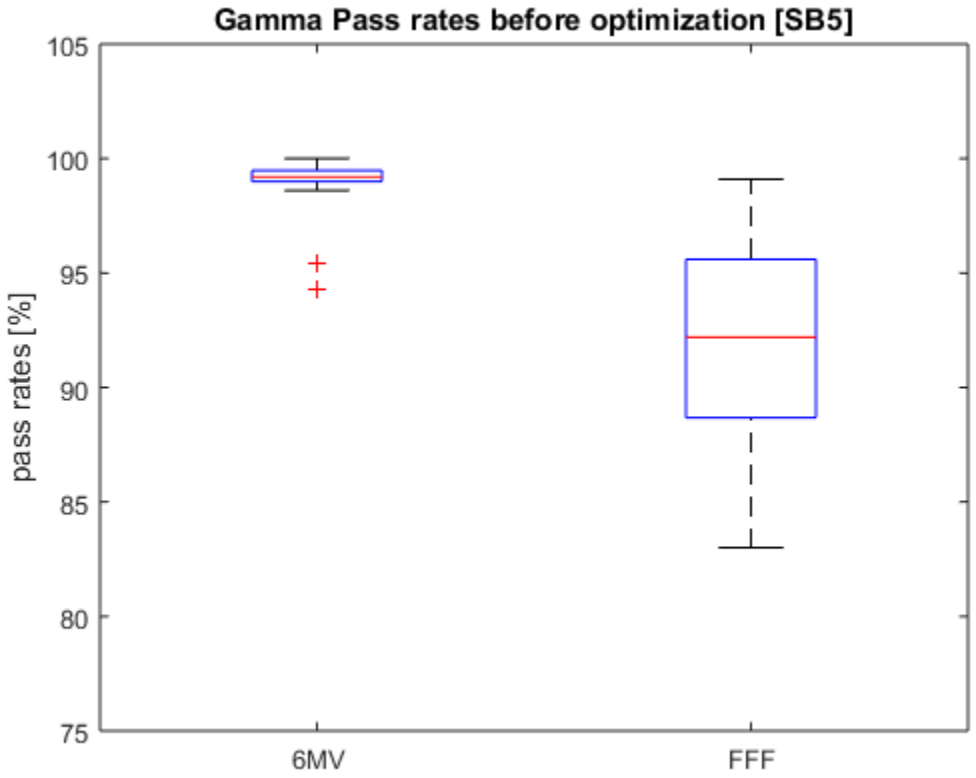

Figure 4.3: Boxplot of the gamma pass rate of 6 MV and FFF before machine optimization of SB5. The upper and lower blue edges of the boxplot represent the 75th and 25th percentiles. The red line represents the median. The red ‘’+’’ indicates possible outliers.

4.2.4 GAMMA PASS RATES FOR 6 MV AND FFF AFTER OPTIMIZATION (SB5)

After machine optimization, there was an increase in the mean total gamma pass rate for the 6 MV plans to 99.9% and a standard deviation of 0.1 and that of the FFF plans had a gamma pass rate of 98.4% and a standard deviation of 2.2. There was significant statistical difference between the 6MV plans and the FFF ($p = 0.000488$). 14 out of the 15 6 MV plans had a perfect gamma pass rate of 100% and the other plan had a pass rate of 99.6%. However, this was not the case for the FFF plans as only 3 out of the 15 plans had a perfect gamma pass rate of 100%.

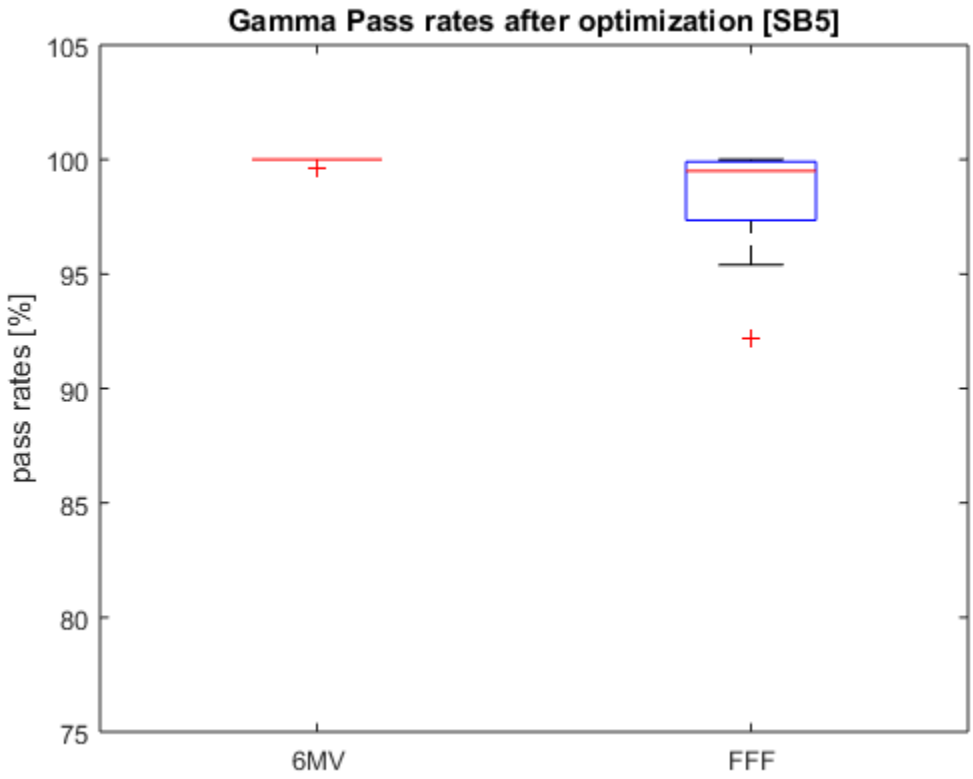

Figure 4.4: Boxplot of the gamma pass rate of 6 MV and FFF after machine optimization of SB5. The upper and lower blue edges of the boxplot represent the 75th and 25th percentiles. The red line represents the median. The red ‘’+’’ indicates possible outliers.

4.2.5 GAMMA PASS RATES FOR 6 MV AND FFF (SB6)

The mean of the total gamma pass rate for SB6 which is the newest of all three linacs used for this study was 99.6% and a 0.5 standard deviation. The corresponding pass rate for the FFF plans was 96.0% and a standard deviation of 2.8. All 6 MV plans had pass rates which met the criteria with 4 individual plans having 100% pass rate. Although all FFF plans also had pass rates satisfying the pass criteria, none of these plans had a 100% pass rate. The

difference between the pass rate of the 6 MV plans and FFF plans was statistically significant (p = 0.0001). The FFF plans are inferior to the 6 MV plans.

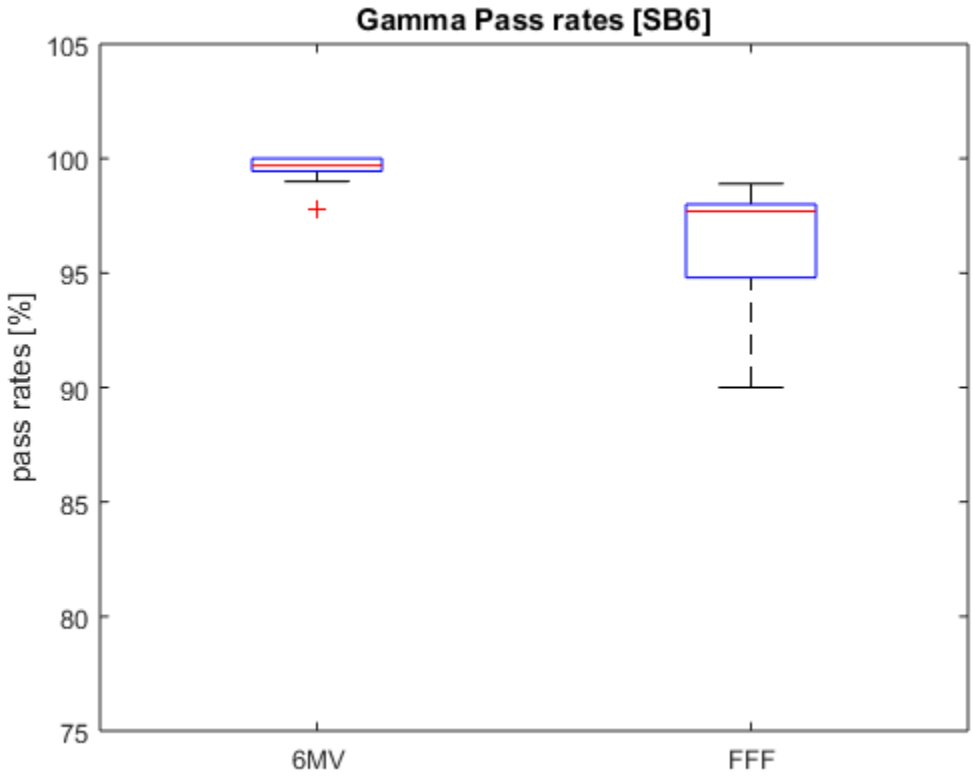

Figure 4.5: Boxplot of the gamma pass rate of 6 MV and FFF (SB6). The upper and lower blue edges of the boxplot represent the 75th and 25th percentiles. The red line represents the median. The red ‘’+’’ indicates possible outlier.

4.2.6 COMAPRISON OF GAMMA PASS RATE FOR SB5 TO PREVIOUS DATA

Also, the pass rate for SB5 before optimization was compared to that of an already existing data from a study conducted in 2018 using the same SB5 linac. From the 2018 data, the mean total gamma pass rate for the 6 MV plan was 98.9% and a standard deviation of 1.8. However, the mean total gamma pass rate for the 6 MV plan for this study was 98.7% with

a standard deviation of 1.6. With respect to the FFF plans for the 2018 data, the mean gamma pass rate was 94.3% and a standard deviation of 4.9 whereas FFF pass rate for this study was 91.7% and a standard deviation of 4.8.

The total gamma pass rates for the 2018 data for 6 MV were not significantly different from the total gamma pass rates for the current data ($p = 0.13$). This was not however the case for the FFF plans for 2018 and the current data where there was statistically significant difference between the gamma pass rates ($p = 0.00$). All the pass rates from all the data set for both 6 MV and FFF plans satisfied the passing criteria.

Table 4.1: The mean and standard deviations of the total gamma pass rates measurement for 6 MV and FFF for both 2018 and current data (SB5).

	6 MV (2018)	6 MV	FFF (2018)	FFF
Mean gamma pass rate (%)	98.9	98.7	94.3	91.7
Standard Deviation	1.8	1.6	4.9	4.8

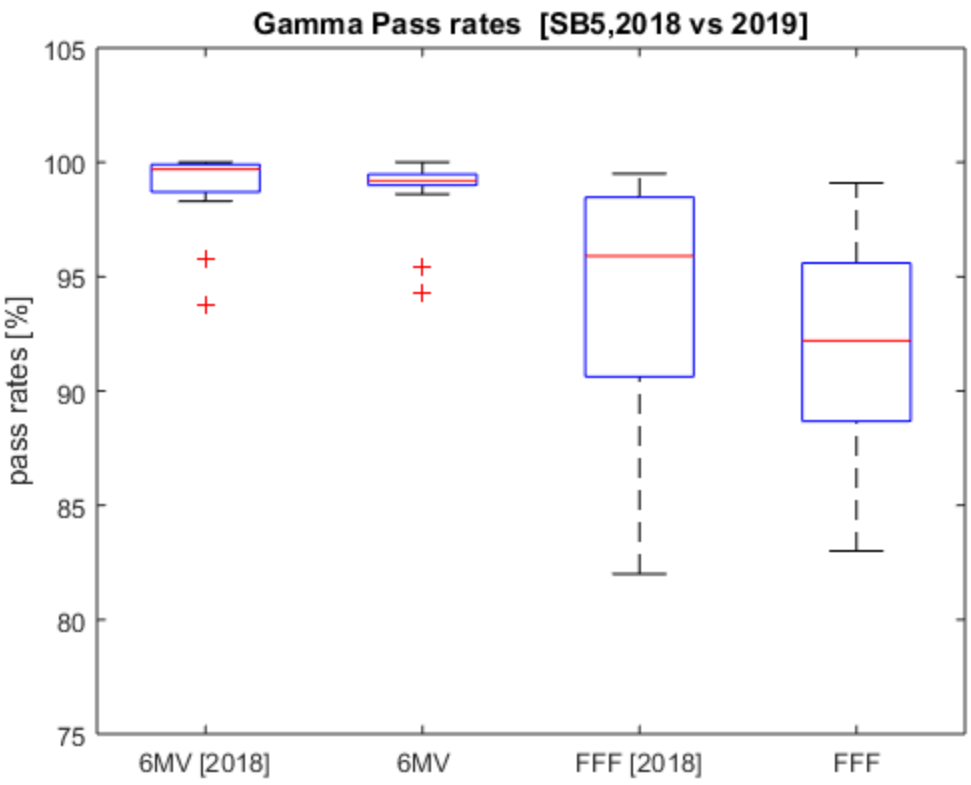

Figure 4.6: Boxplot of the gamma pass rate of 6 MV and FFF plans for both 2018 data and current data. The upper and lower blue edges of the boxplot represent the 75th and 25th percentiles. The red line represents the median. The red ‘’+’’ indicates possible outliers.

From figure 4.6 above, it can be observed that the gamma pass rates for 2018 6 MV plans was almost the same as that of the current data but for the FFF plan, the pass rate for the 2018 plan had a somewhat higher pass rate than the current.

4.2.7 COMPARISON OF THE GAMMA PASS RATES FOR ALL 3 LINACS FOR BOTH 6 MV AND FFF PLANS.

The gamma pass rates for all the 3 linacs was compared to find out which of these linacs could accurately deliver VMAT plans for both 6 MV and FFF. The parameters used for this comparison was the gamma pass rates for SB6 and pass rates after optimization for both SB3 and SB5 since it has been shown that the pass rates after machine optimization is higher than before optimization.

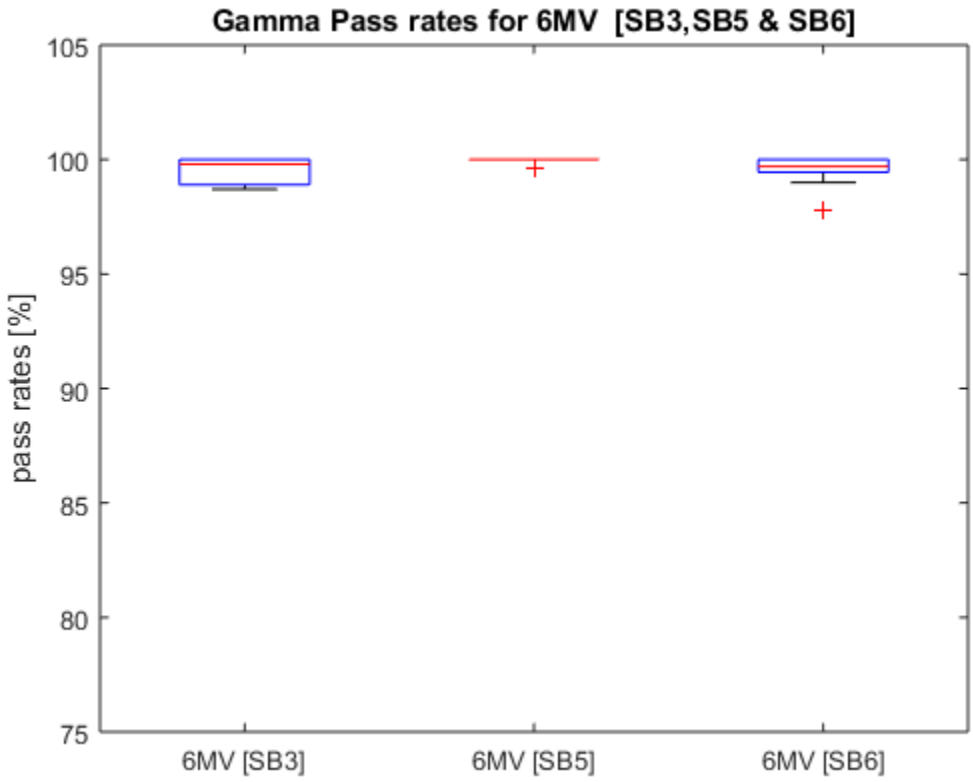

Figure 4.7: Boxplot comparing the gamma pass rate of 6 MV SB3, SB5 and SB6. The upper and lower blue edges of the boxplot represent the 75th and 25th percentiles. The red line represents the median.

There was significant difference between the gamma pass rates using SB3 and SB5 for 6 MV plans (p = 0.01). From figure 4.7, SB5 produced a higher pass rate than SB3. Also, there was significant difference between the pass rates of SB5 and SB6 (p = 0.01). However, there was no significant difference that of SB3 and SB6 (p = 0.72). It can therefore be said that the SB5 linac is better at delivering 6MV plans more accurately than SB6 and SB3 in that order since the mean pass rates for SB5, SB6 and SB3 were 99.9%, 99.6% and 92.9% respectively.

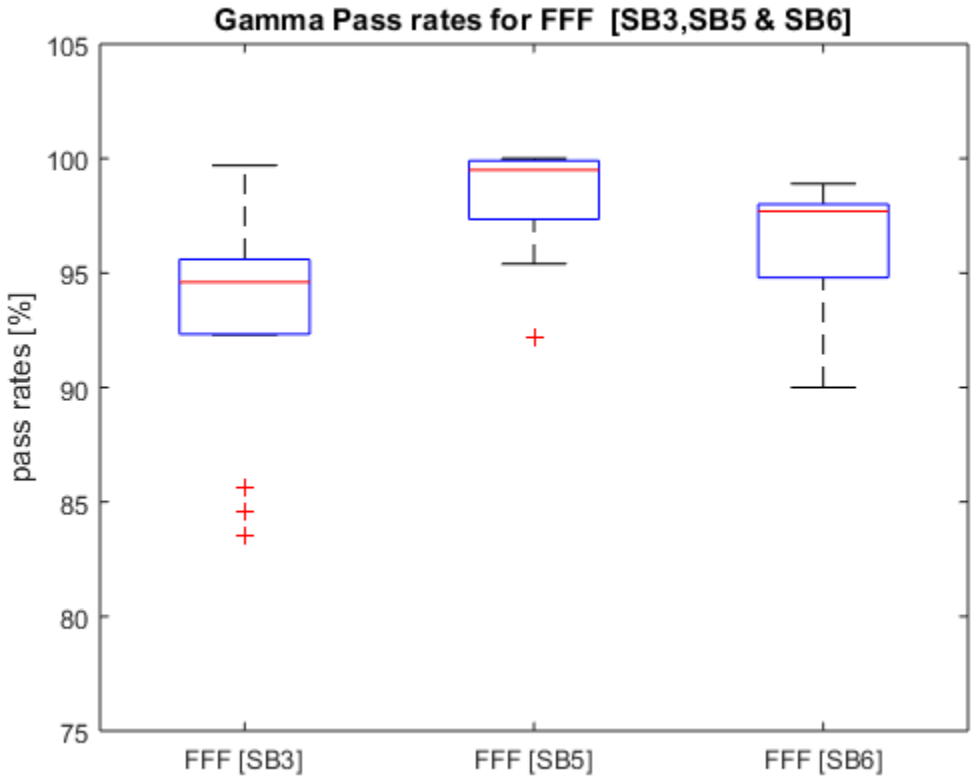

Figure 4.8: Boxplot comparing the gamma pass rate of FFF SB3, SB5 and SB6. The upper and lower blue edges of the boxplot represent the 75th and 25th percentiles. The red line represents the median. The red ‘’+’’ represents possible outliers.

With regards to FFF plans, it was observed that SB5 was the best linac to accurately deliver FFF treatment plans. The mean pass rates produced from SB5, SB6 and SB3 were respectively 98.4, 96.0 and 93.1%. Also, SB3 was inferior to SB6 in delivering the FFF plans. There was significant difference ($p = 0.0008$) observed between SB3 and SB5. No significant difference ($p = 0.07$) in pass rates was observed between SB3 and SB6. A significant difference between SB5 and SB6 was observed ($p = 0.01$).

Comparing figure 4.7 and 4.8 shows that conventional flattening filtered beams are able to deliver cervical cancer VMAT plans more accurately than flattening filter free beams (FFF). Similar finding was reported by (Balik et al., 2018) where it was concluded that FFF generates inferior homogenous dose distributions compared to conventional flattened beams. However, (Lu et al., 2016) reported that using FFF in sinonasal cancer treatment produced a better dose distribution than the flattened beam.

4.2.8 INDIVIDUAL GAMMA PASS RATES

Comparison was made between pass rates of 6MV and FFF plans for individual patient's plan to verify if some individual FFF plans performed better than their corresponding 6MV plans. This was done using data from the pass rates of SB6 and after optimization of SB3 and SB5.

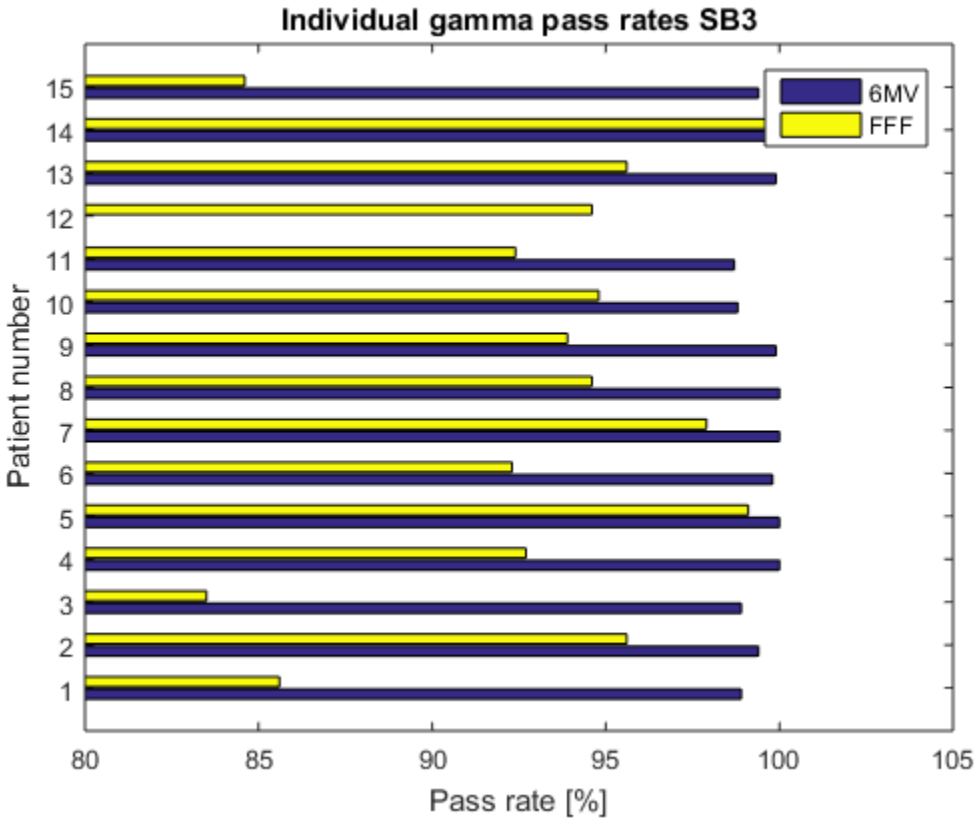

Figure 4.9: Bar chart showing individual gamma pass rates of both 6 MV and FFF plans from SB3.

From the figure above, all 6 MV plans had higher pass rates than the FFF plans. With the exception of plan 12 where the 6 MV plan was complex for the multileaf and hence the plan could not be implemented.

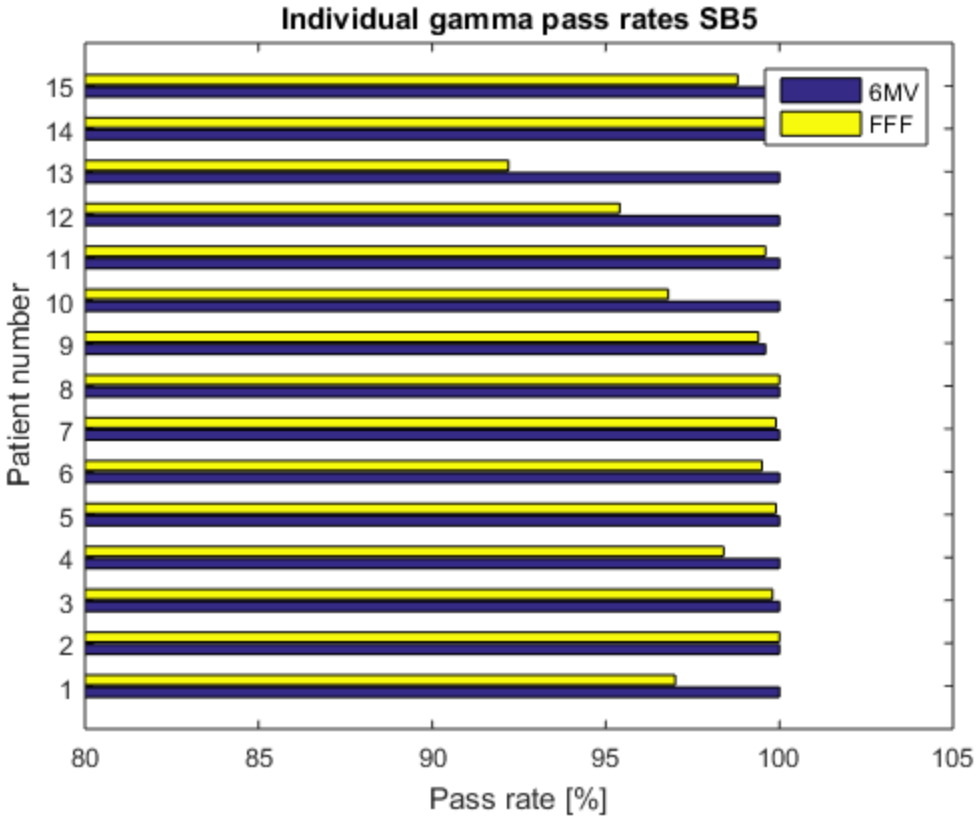

Figure 4.10: Bar chart showing individual gamma pass rates of both 6 MV and FFF plans from SB5. All 6 MV plans had a higher pass rate than the FFF plans.

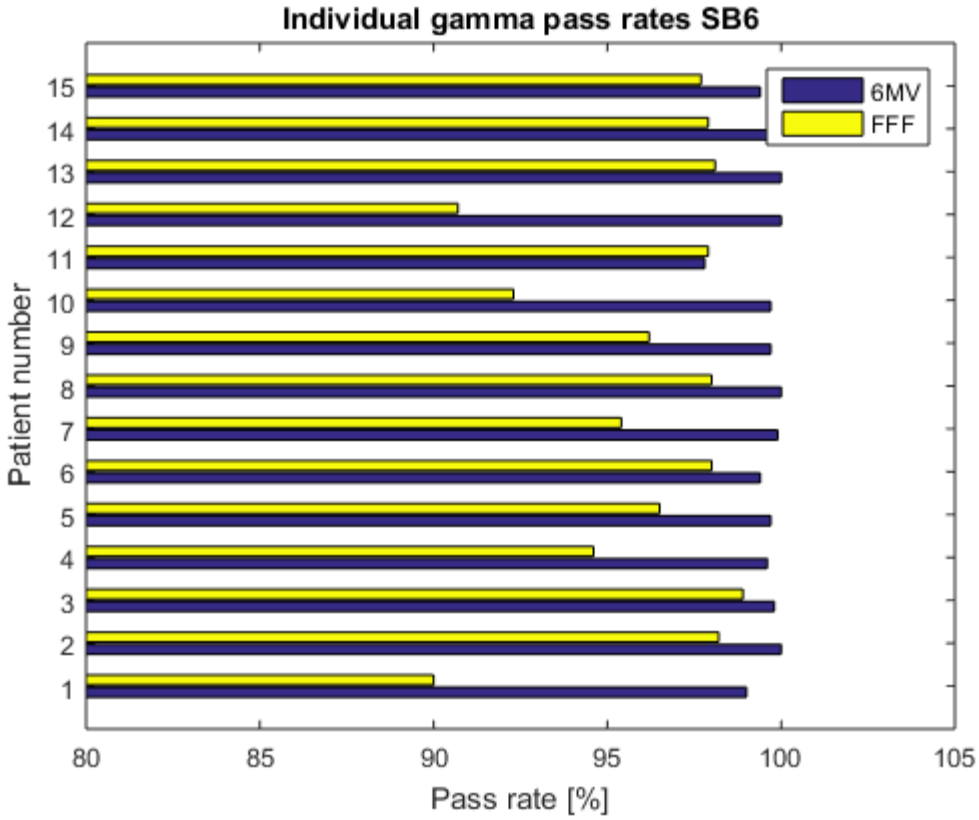

Figure 4.11: Bar chart showing individual gamma pass rates of both 6MV and FFF plans from SB6. All 6MV plans had a higher pass rate than the FFF plans.

4.3 MONITOR UNITS (MU's)

The mean monitor unit for the 6 MV plans was 506.3 MU and a standard deviation of 48.6 while that of the FFF plans had a mean MU of 701.5 with a standard deviation of 87.6. The total monitor units (MUs) for the FFF plans were significantly greater than the 6MV plans ($p = 6.1x10^{-5}$). This is in agreement with (Kumar et al., 2017) where it was also concluded that FFF plans require more numbers of monitor units in comparison to conventional filtered beams. They reported that there was an increase of 20.5% and 43.7% in MUs for FFF of 6 and 10MV respectively in comparison to flattened beams of 6 and 10 MV.

Increased monitor units for FFF compared to conventional flattened beams was also reported by (Rout et al., 2014). Also, increased number of MUs was observed for the use of FFF beams compared with conventional flattened beams (Lu et al., 2016).

One reason for this could be due to the fact that FFF beams are inhomogeneous and therefore requires more modulation thus increasing the MU. Intensity of FFF beam decreases sharply with off-axis distance for field sizes larger than and equal to 10x10cm^2 hence, requires the off-axis distance-dependence modulation of FFF photon beam. This requires large number of MUs to deliver radiation dose to the tumor (Sharma, 2011).

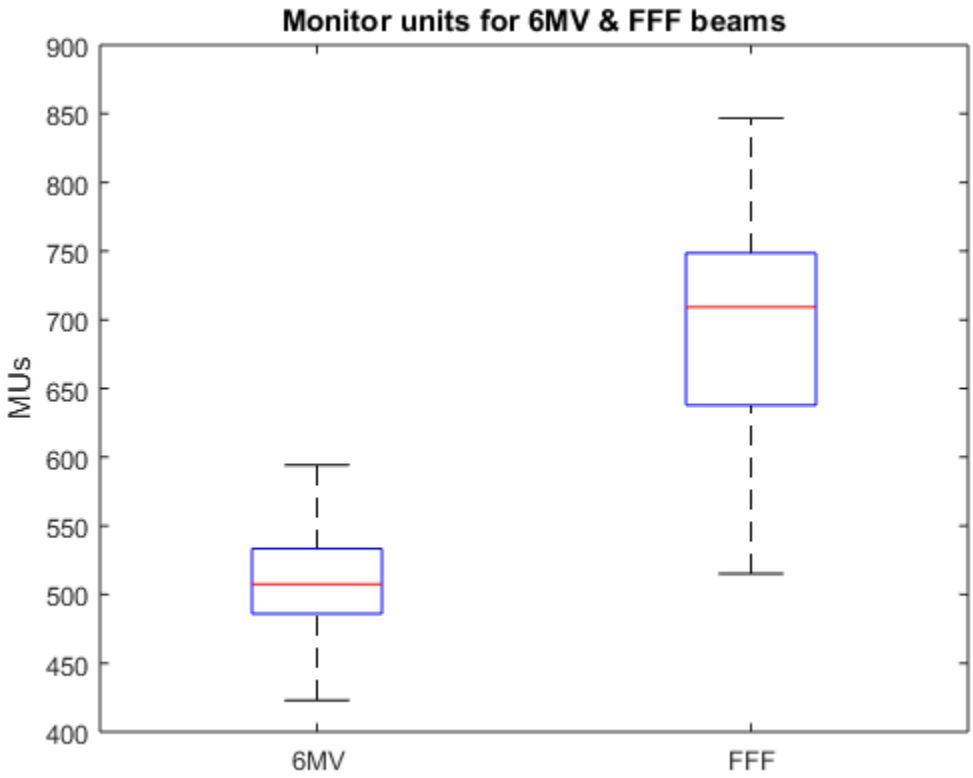

Figure 4.12: Boxplot of monitor units for both 6 MV and FFF plans

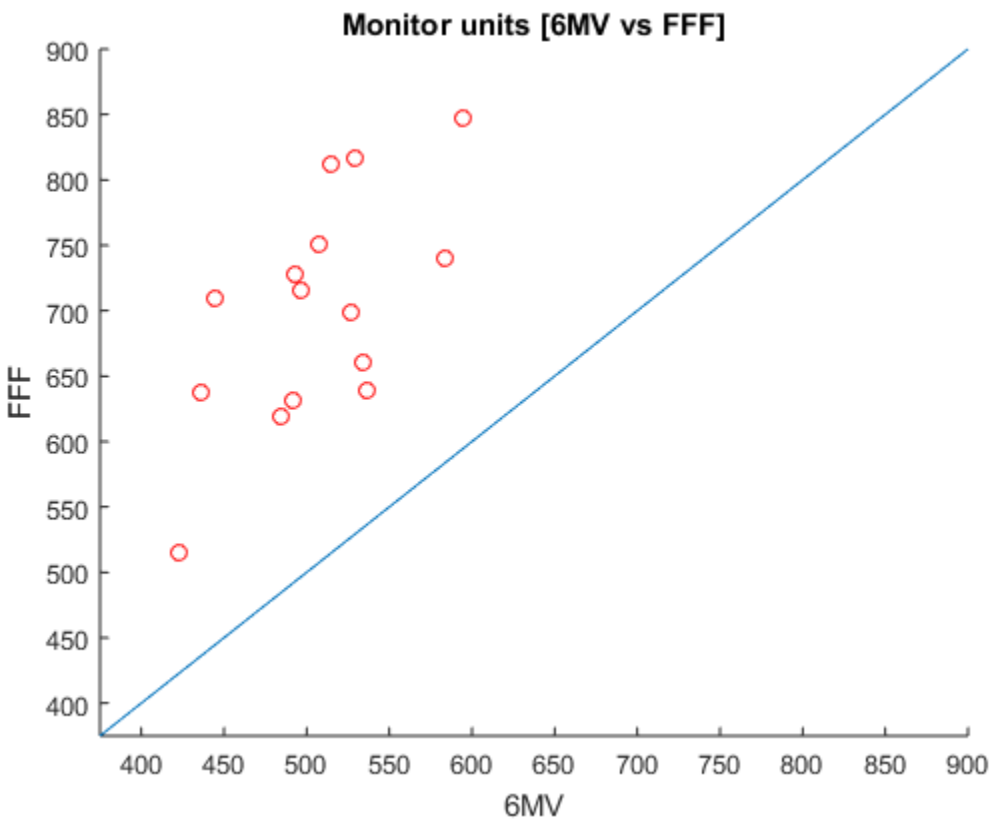

Figure 4.13: Scatter plot of MUs of 6 MV versus (vs) FFF plans. The blue line represents a unity line (x = y). The red points lying above the blue line means that all FFF plans had higher monitor units than the 6 MV plans.

4.3.1 MONITOR UNIT AND GAMMA PASS RATE

Since the gamma pass rate after machine optimization of SB5 was higher than all the other linacs used for this study, it was chosen and compared to the monitor units for both 6 MV and FFF plans.

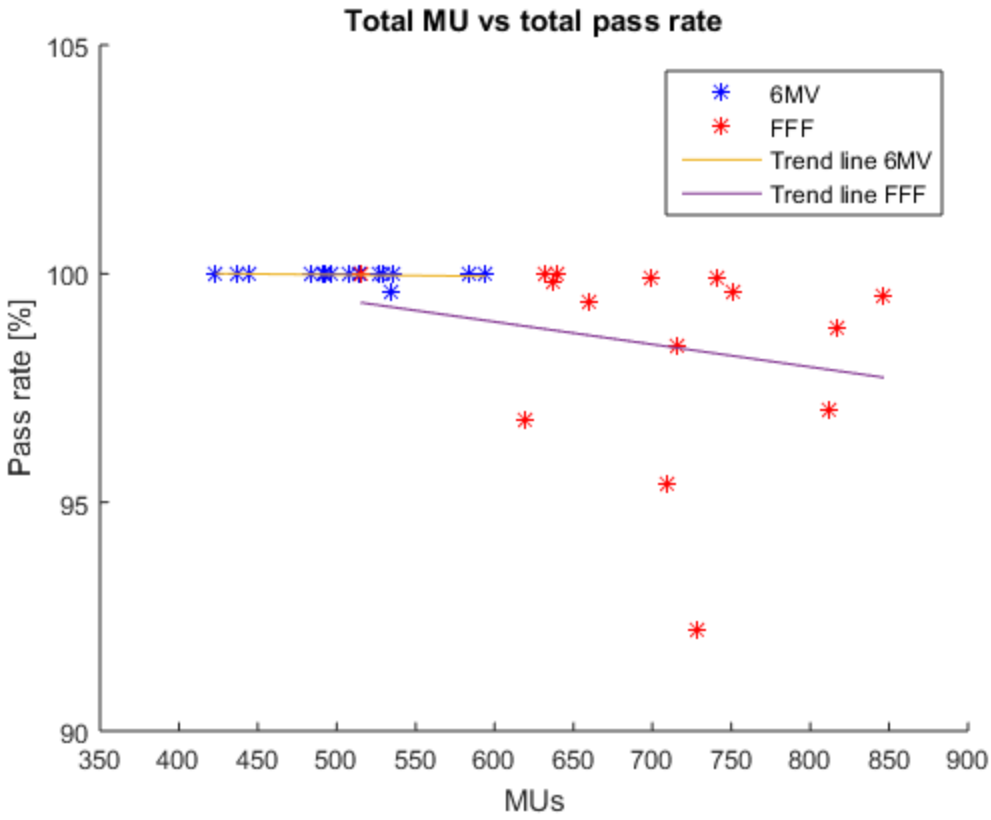

Figure 4.14: Scatter plot of the total monitor unit versus the total gamma pass rates for 6 MV and FFF plans (SB5).

As MU increased for 6 MV plans, it was observed that the pass rate was relatively constant (100% pass rate). This means that increasing the monitor unit for 6 MV plans have little or no effect on the gamma pass rate. The situation was however different for the FFF plans where increasing MU was found to decrease the gamma pass rate for FFF plans. This could be due to the fact that rapid modulation of the multileaf collimator is needed when using flattening filter free beam. Dose rate increases in FFF mode and therefore, it would require a longer MU to deliver the radiation dose. The pass rate for the FFF becomes scattered as MU increases.

4.4 VOLUME OF PTV AND GAMMA PASS RATE

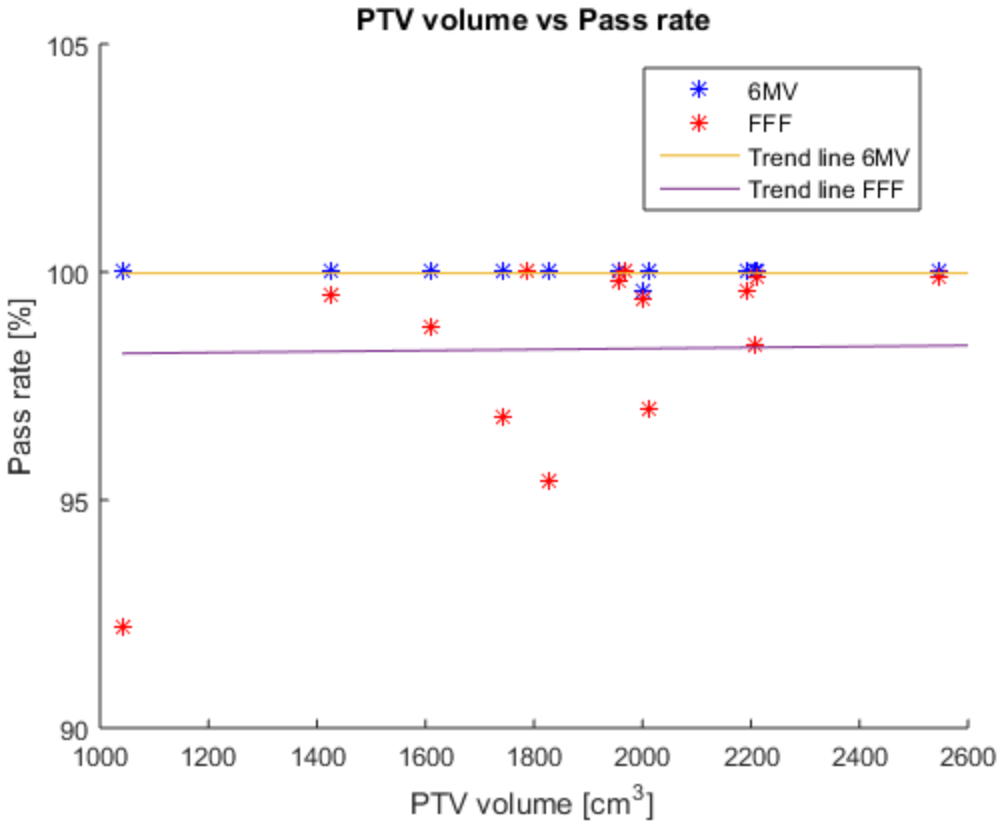

Figure 4.15: Scatter plot of PTV volumes versus the gamma pass rate for 6 MV and FFF plans (SB5).

It can be observed from the figure above that as the volume of the PTV increased, there was no reduction in the pass rate for the 6 MV plans. Most individual 6 MV plans had a 100% gamma rate even as PTV volume increased. The pass rate for FFF plans was also constant as the planning target volume increased. Based on the figure above, it can be said that increasing planning target volumes have no effect on the gamma pass rates for both 6 MV and FFF plans because the pass rate remains constant.

4.5 ANALYSIS OF MEDIAN FOR 6MV AND FFF

The median value is generated by the Scandidos software during gamma analysis and ideally the median value should be zero. This signifies how the dose deviates from the center of the phantom. However, due to deviations and errors, attaining a median value of zero is almost impossible. Hence it is acceptable or best if the median value is closer to zero. A comparison of the median values was therefore made between 6 MV plans and FFF plans using data from SB5 after machine optimization.

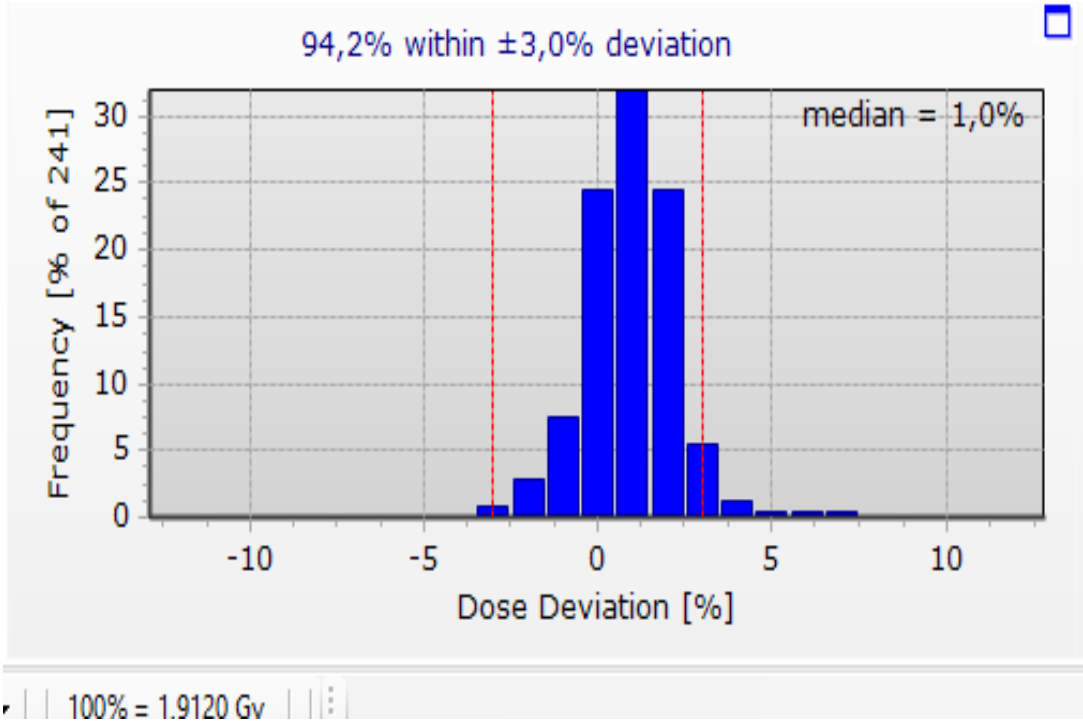

Figure 4.16: A graph showing the median and dose deviation obtained from the Scandidos Delta4 software.

Table 4.2: Median values for both 6 MV and FFF plans

PLANS	6 MV	FFF
PT1	0.10	0.70
PT2	-0.20	0.30
PT3	-0.20	0.50
PT4	0.00	0.50
PT5	-0.20	0.20
PT6	-0.20	0.30
PT7	-0.40	0.30
PT8	-0.30	0.30
PT9	-0.10	0.40
PT10	0.40	0.40
PT11	0.80	0.70
PT12	0.10	0.50
PT13	-0.20	1.40
PT14	-0.40	0.10
PT15	0.00	0.60

The mean of the Median for 6 MV was -0.05 and a standard deviation of 0.32 while that of the FFF plans had a mean of 0.48 and a standard deviation of 0.31. Based on this, the 6 MV plans had values for median which is closest to zero.

CHAPTER FIVE

5 CONCLUSION AND RECOMMENDATIONS

5.1 CONCLUSION

Based on measurements on 3 Elekta linacs, 6 MV VMAT plans with conventional flattened beams are delivered more accurately and hence more beneficial compared to flattening filter free (FFF) VMAT plans for external radiation of cervical cancer with affected pelvic lymph nodes. The results are visualized in that the 6 MV plans for the 15 patients generally produced a higher gamma pass rate than the corresponding FFF plans for the same patients.

The study also visualized that there were individual differences in the delivery of the treatment plans between the 3 linacs tested. It is also visualized that gamma pass rates improved remarkably after machine optimization of all three linacs. Also, not all VMAT treatment plans are technically feasible or can be delivered by one of the linear accelerator tested, although they could be delivered by the two other equal linacs tested.

This study also concludes that the volume of PTVs do not change the gamma pass rate for either 6 MV or FFF plans. Also, larger MU seem to reduce the pass rate for FFF plans. For lower MUs, the difference in pass rates are smaller.

5.2 RECOMMENDATIONS

The following recommendations are made to personnel involved in the whole radiotherapy and treatment planning process including medical physicists, dosimetrists, radiation and medical oncologists and radiotherapists.

1. All VMAT plans should be verified using the appropriate phantom to compare the planned and measure dose distributions before treatment is delivered to the patient.
2. There is the need for regular maintenance of linear accelerators.
3. Radiotherapy centers should include the recommendations from EMBRACE II study into their protocols for cervical cancer treatment.

5.2.1 RECOMMENDATION FOR FURTHER RESEARCH WORK

A tighter gamma pass rate criteria such as 2%2mm or 2%1mm could be used for further studies. VMAT plans for the other cancers such as head and neck, lungs, prostate and cancers of the gastrointestinal tract. Factors other than the effect of MU and volume of PTV on pass rates could also be studied.

REFERENCES

AAPM, T. (2009). *IMRT & VMAT Quality Assurance*. Retrieved from Med Phys:

Abolaban, F., Zaman, S., & Cashmore, J. (2016). Changes in Patterns of Intensity-modulated Radiotherapy Verification and Quality Assurance in the UK. *Clin Oncol (R Coll Radiol), 28*(8), e28-34. doi:10.1016/j.clon.2016.01.013

Abshire, D., & Lang, M. K. (2018). The Evolution of Radiation Therapy in Treating Cancer. *Semin Oncol Nurs, 34*(2), 151-157. doi:10.1016/j.soncn.2018.03.006

Adli, M., Mayr, N. A., Kaiser, H. S., Skwarchuk, M. W., Meeks, S. L., Mardirossian, G., & (2003). Does prone positioning reduce small bowel dose in pelvic radiation with intensity-modulated radiotherapy for gynecologic cancer? *Int J Radiat Oncol Biol Phys, 57(1):230-238.*

Agnew, C. E., & McGarry, C. K. (2016). A tool to include gamma analysis software into a quality assurance program. *Radiother Oncol, 118*(3), 568-573. doi:10.1016/j.radonc.2015.11.034

Akartunalı, K., Mak-Hau, V., Tran, T., & A unified mixed-integer programming model for simultaneous fluence weight and aperture optimization in VMAT, T., and Cyberknife. Computers & Operations Research 2015;56:134-150. (2015). A unified mixed-integer programming model for simultaneous fluence weight and aperture optimization in VMAT, Tomotherapy, and Cyberknife. . *Computers & Operations Research*

56:134-150.

Alber, M. M., Broggi, S., Wagter, C., Eichwurzel, I., Engström, P., & Fiorino, C. (2008). Guidelines for the Verification of IMRT. *ESTRO, 10.1016/S0167*.

Allison, L. M. (2013). *Evaluating Pre-Treatment IMRT &VMAT QA Techniques Using Receiver Operating Characteristic (ROC) Analysis.* (Masters Degree), Duke University, UK.

Alvarez, M. J., & Fabian, P. (2010). Evaluation of volumetric modulated arc therapy (VMAT) with Oncentra MasterPlan® for the treatment of head and neck cancer. *Radiation Oncology*

5:110.

Baldock, C., De Deene, Y., Doran, S., Ibbott, G., Jirasek, A., & Lepage, M. (2010). Polymer gel dosimetry. *Phys Med Biol, 55(5).*

Balik, S., Qi, P., Magnelli, A., Chao, S. T., Suh, J. H., & Zhuang, T. (2018). Comparison of Spine SRS VMAT plans with Flattening Filter Free 6 MV or 10 MV beams. *International Journal of Radiation Oncology*Biology*Physics, 102*(3). doi:10.1016/j.ijrobp.2018.07.1436

Bats, A. S., Buénerd, A., & Querleu, D. (2011). Diagnostic value of intraoperative examination of sentinel lymph node in early cervical cancer: A prospective, multicenter study. . *Gynecol Oncol., 123(2):230–235*.

Baumer, C., Geismar, D., Koska, B., Kramer, P. H., Lambert, J., Lemke, M., . . . Vermeren, X. (2017). Comprehensive clinical commissioning and validation of the RayStation treatment planning system for proton therapy with active scanning and passive treatment techniques. *Phys Med, 43*, 15-24. doi:10.1016/j.ejmp.2017.09.136

Bedford, J. L., Lee, Y. K., Wai, P., South, C. P., & Warrington, A. P. (2009). Evaluation of the Delta4 phantom for IMRT and VMAT verification. *Phys Med Biol, 54*(9), N167-176. doi:10.1088/0031-9155/54/9/N04

Berger, T., Seppenwoolde, Y., Potter, R., Assenholt, M. S., Lindegaard, J. C., Nout, R. A., . . . Group, E. C. (2019). Importance of Technique, Target Selection, Contouring, Dose Prescription, and Dose-Planning in External Beam Radiation Therapy for Cervical Cancer: Evolution of Practice From EMBRACE-I to II. *Int J Radiat Oncol Biol Phys, 104*(4), 885-894. doi:10.1016/j.ijrobp.2019.03.020

Boutevin, F., Feuillade, J., Gautier, M., Diagne, M., & Dejean, C. (2013). Influence of the collimator rotation and the position of the isocenter on quality controls of treatment plans in dynamic arctherapy. *Physica Medica, 29*. doi:10.1016/j.ejmp.2013.08.112

Bowers, D., House, A., & H., D. (2011). Getting Started in Health Research. *John Wiley & Sons*.

Capomolla, C., Zagari, A., Quarta, S., Luca, D. D., Carlà, A., Cazzato, M., & Martinucci, E. (2018). 131 Performance analysis of new Delta4 Phantom+ using Flattening-Filter and Flattening Filter-Free beams. *Physica Medica, 56*. doi:10.1016/j.ejmp.2018.04.142

Chen, Z., d'Errico, F., & Nath, R. (2006). Principles and requirements of external beam dosimetry. *Radiation Measurements, 41*, S2-S21. doi:10.1016/j.radmeas.2007.01.010

Chieregato, M., M. Galelli, M., S. , S.R., K., Bassetti, C., & Donadoni, L. (2018). Low modulated 6 MV Flattening Filter Free Intensity Modulated Radiation Therapy (FFF-IMRT) for left breast treatments with Active Breath CoordinatorTM (ABC): A feasibility study

Physica Medica, 56:133-278.

Cihoric, N., Tsikkinis, & Tapia, A. C. (2015). Dose escalated intensity modulated radiotherapy in the treatment of cervical cancer. *Radiat Oncol, 10:240*.

Cirino, E. T., Iftimia, I., & Lo, T. C. (2012). Using Dose Homogeneity Index and Conformity Index to Evaluate Prostate High-dose-rate Plan Quality and Consistency. *International Journal of Radiation Oncology*Biology*Physics, 84*(3), S770-S771. doi:10.1016/j.ijrobp.2012.07.2062

Cohen, P. A., Jhingran, A., Oaknin, A., & Denny, L. (2019). Cervical cancer. *The Lancet, 393*(10167), 169-182. doi:10.1016/s0140-6736(18)32470-x

Collins, S. P., Coppa , N. D., Zhang, Y., Collins, B. T., McRae, D. A., & Jean, W. C. (2006). Cyberknife radiosurgery in the treatment of complex skull base tumors: Analysis of treatment planning parameters. *Radiat Oncol., 1:46*.

Dixon, P., & O'Sullivan, B. (2002). Radiotherapy Quality assurance: time for everyone to take it seriously. *European Journal of Cancer, 39 423-429*.

Du, R., Li, L., Ma, S., Tan, X., Zhong, S., & Wu, M. (2018). Lymph nodes metastasis in cervical cancer: Incidences, risk factors, consequences and imaging evaluations. *Asia Pac J Clin Oncol, 14*(5), e380-e385. doi:10.1111/ajco.12997

Dursun, P., Taşkın, Z. C., & Altınel, İ. K. (2016). Mathematical Models for Optimal Volumetric Modulated Arc Therapy (VMAT) Treatment Planning. *Procedia Computer Science, 100*, 644-651. doi:10.1016/j.procs.2016.09.206

Esch, A. V., Bogarets, R., Kutcher, G. J., & Huyskens, D. (2000). Quality assurance in radiotherapy by identifying standardsand monitoring treatment preparatiom. *Radiotherapy and Oncology, 56(2000) 109-115*.

Essers, M., Langen, M., Dirkx, M. L., & (2001). Commissioning of a commercially available system for intensity-modulated radiotherapy dose delivery with dynamic multileaf collimation.

. *Radiother Oncol, 60:215–224.*

Fontaine, J., Taecsh, F., Djibo-Sidikou, A., Bertosi, A., & Retif, P. (2018). 11 Evaluation of delivery analysis software (Accuray), comparison to Delta 4 Phantom. *Physica Medica, 56*, 7-8. doi:10.1016/j.ejmp.2018.09.024

Fowble, B., Hanlon, A., Freedman, G., & (2000). Internal mammary node irradiation neither decreases distant metastases nor improves survival in stage I and II breast cancer. *Int J Radiat, 47, 883–894*.

Georg, D., Knöös, T., McClean, B., & (2011). Current status and future perspective of flattening filter free photon beam. *Med Phys, 38(March (3)):1280–93*.

Georges, N., Jean-Jacques, M., & Pierre, B. (2006). Conformity index: A review. *Int J Radiation Oncology Biol Phys. , 64(2):333–342*.

Groenen, M., Verhagen, C., Snyers, A., Verhoef, C., & Van Leeuwen, R. (2018). PO-1074: Pinnacle Auto-Planning using EMBRACE II guidelines for EBRT of cervix carcinoma; clinical experience. *Radiotherapy and Oncology, 127*, S604-S605. doi:10.1016/s0167-8140(18)31384-7

Halperin, E. C., Perez, C. A., & Brady, L. W. (2008). *Perez and Brady's principles and practice of radiation oncology (5th ed.)* (Vol. 5th ed): Lippincott Williams & Wilkins.

Han, C., Liu, A., Liang, J., Da Silva, A., Zhang, S., & Wong, J. Y. C. (2018). Dosimetric Evaluation of Treatment Plans for a Biology-Guided Radiation Therapy System in

Treatment of Nasopharyngeal Cancer. *International Journal of Radiation Oncology*Biology*Physics, 102*(3). doi:10.1016/j.ijrobp.2018.07.1482

Hartford, A. C. (2012). Practice Guidelines for Intensity Modulated Radiatio Therapy (IMRT). *American journal of clinical oncology, 35(6): p. 612-617.*

Hata, M., Koike, I., Miyagi, E., Numazaki, R., Asai-Sato, M., Kasuya, T., . . . Inoue, T. (2013). Radiation therapy for pelvic lymph node metastasis from uterine cervical cancer. *Gynecol Oncol, 131*(1), 99-102. doi:10.1016/j.ygyno.2013.07.085

Hielemann, G., Poppe, B., & Laub, W. (2013). On the sensitivity of common gamma-index evaluation methods to MLC misalignments in Rapidarc quality assurance. *Crossmark.*

Higby, C., Khafaga, Y., Al-Shabanah, M., Mousa, A., Ilyas, M., Nazer, G., & Khalil, E. M. (2016). Volumetric-modulated arc therapy (VMAT) versus 3D-conformal radiation therapy in supra-diaphragmatic Hodgkin's Lymphoma with mediastinal involvement: A dosimetric comparison. *J Egypt Natl Canc Inst, 28*(3), 163-168. doi:10.1016/j.jnci.2016.04.007

Hoffmann, M., Pacey, J., Goodworth, J., Laszcyzk, A., Ford, R., Chick, B., . . . Westhuyzen, J. (2019). Analysis of a volumetric-modulated arc therapy (VMAT) single phase prostate template as a class solution. *Rep Pract Oncol Radiother, 24*(1), 92-96. doi:10.1016/j.rpor.2018.10.009

Holt, A., van Vliet-Vroegindeweij, C., Mans, A., Belderbos, J. S., & Damen, E. M. (2011). Volumetric-modulated arc therapy for stereotactic body radiotherapy of lung tumors: a comparison with intensity-modulated radiotherapy techniques. *Int J Radiat Oncol Biol Phys, 81*(5), 1560-1567. doi:10.1016/j.ijrobp.2010.09.014

Hoskin, P., Clark, C. H., & (2006). Radiotherapy in practice external beam therapy. *Oxford University Press*.

Huang, B. T., Lin, Z., Lin, P. X., Lu, J. Y., & Chen, C. Z. (2015). Monitor unit optimization in stereotactic body radiotherapy for small peripheral non-small cell lung cancer patients. *Sci Rep, 5:18453*.

Hurkamns, C. W., Remeijer, P., Lebesque, J. V., Mijnheer, B. J., Set-up, verification using portal imaging: Review of current clinical practice, R. O., & 105–226. (2001). Set-up verification using portal imaging: Review of current clinical practice. *Radiother. Oncol.*

, 58:105–226.

Hussein, M., Rowshanfarzad, P., Ebert, M. A., & Nisbet, A. (2013). A comparison of the gamma index analysis in various commercial IMRT/VMAT QA systems.

. Radiother Oncol, 109:370–6.

Hussein, M., Rowshanfarzad, P., Ebert, M. A., Nisbet, A., Clark, C. H., & (2013). A comparison of the gamma index analysis in various commercial IMRT/VMAT QA systems.

. Radiother Oncol., 109:370–6.

Jimenez-Puertas, S., Sanchez-Artunedo, D., & Hermida-Lopez, M. (2018). Assessment of the Monitor Unit Objective tool for VMAT in the Eclipse treatment planning system. *Rep Pract Oncol Radiother, 23*(2), 121-125. doi:10.1016/j.rpor.2018.02.001

Kataria, T., Sharma, K., Subramani, V., Karrthick, K. P., & Bisht , S. S. (2012). Homogeneity Index: An objective tool for assessment of conformal radiation treatments. *J Med Phys., 37(4): 207–213*.

Kerby, D. (2014). The simple difference formula: An approach to teaching nonparametric correlation. *Comprehensive Psychology, 3*.

Kragl, G., Wetterstedt, S., Knausl, B., & (2009). Dosimetric characteristics of 6 and 10 MV unflattened photon beams. *Radiother Oncol, 93:141–6*.

Kumar, L., Yadav, G., Samuvel, K. R., Bhushan, M., Kumar, P., Suhail, M., & Pal, M. (2017). Dosimetric influence of filtered and flattening filter free photon beam on rapid arc (RA) radiotherapy planning in case of cervix carcinoma. *Rep Pract Oncol Radiother, 22*(1), 10-18. doi:10.1016/j.rpor.2016.09.010

Kung, J. H., Reft, C., Jackson, W., & Abdalla, I. (2001). Intensity-modulated radiotherapy for a prostate patient with a metal prosthesis. *Med. Dosim, 26 (4), 305–308.*

.

Lalit, K., Girigesh, Y., Kothanda, R., Manindra, B., & Pawan, K. (2017). Dosimetric influence of filtered and flattening filter free photon beam on rapid arc (RA) radiotherapy planning in case of cervix carcinoma

Rep Pract Oncol Radiother. doi:10.1016/j.rpor.2016.09.010

Li, Z., Yang, S., Liu, L., & ., H. S. (2013). A comparison of concurrent chemoradiotherapy and radiotherapy in Chinese patients with locally advanced cervical carcinoma:a multi-center study. *Radiat Oncol, 9:212*.

Lievens, Y., Verstraete, J., Pauwels, K., & Bogaert, W. (2009). Time and motion study of radiotherapy delivery: economic burden of increased quality assurance and IMRT. *Radiother Oncol, 93:137–40*.

Ling, C. C., Zhang, P., Archambault, Y., Bocanek, J., Tang, G., Lasasso, T., . . . 2008;72:575–81., O. B. P. (2008). Commissioning and quality assurance of RapidArc radiotherapy delivery system. *Int J Radiat Oncol Biol Phys, 72:575–81*.

Liu, Z., Hu, K., Liu, A., Shen, J., Hou, X., Lian, X., . . . Zhang, F. (2016). Patterns of lymph node metastasis in locally advanced cervical cancer. *Medicine (Baltimore), 95*(39), e4814. doi:10.1097/MD.0000000000004814

Low, A. (2003). Evaluation of the gamma dose distribution comparison method. *Med Phys, 30*(9), 2455-2464. doi:10.1118/1.1598711

Low, D. A., Harms, W. B., Mutic, S., & Purdy, J. A. (1998). A technique for the quantitative evaluation of dose distributions *Med Phys, 25:656-661*.

Lu, J. Y., Zheng, J., Zhang, W. Z., & Huang, B. T. (2016). Flattening Filter-Free Beams in Intensity-Modulated Radiotherapy and Volumetric Modulated Arc Therapy for Sinonasal Cancer. *PLoS One, 11*(1), e0146604. doi:10.1371/journal.pone.0146604

Lutgens, L. C. D., N.E. , Gueulette, J., Cleutjens, J. P., Berger, M. P., Wouters, B. G., Meyenfeldt, M. F., & Lambin, P. (2003). A physiologic marker enabling quantitation and monitoring of epithelial radiation-induced small bowel damage. *Int J Radiat Oncol Biol Phys. , 57(4):1067-74.*

Ma, C., SB, J., T, P., Y, C., JS, L., & J, D. (2003). A quality assurance phantom for IMRT dose verification. *Phys Med Biol, 48:561-72*.

Machichi, M., Oulhouq, Y., Rrhioua, A., Zerfaoui, M., & Bakari, D. (2019). Simulation of the dose calculation and distribution in radiation Therapy Treatment Planning System. *Materials Today: Proceedings, 13*, 982-990. doi:10.1016/j.matpr.2019.04.063

Marcu, L., Bezak, E., & Allen, B. (2012). Biomedical Physics in Radiotherapy for Cancer. *Springer Science and Business Media B.V.*

McNiven, A., Kron, T., & Van Dyk, J. (2004). A multileaf collimator phantom for the quality assurance of radiation therapy planning systems and CT simulators. *Int J Radiat Oncol Biol Phys, 60*(3), 994-1001. doi:10.1016/j.ijrobp.2004.06.013

Mohamed, I. E., Ibrahim, A. G., Zidan, H. M., El-Bahkiry, H. S., & El-sahragti, A. Y. (2018). Physical dosimetry of volumetric modulated arc therapy (VMAT) using EPID and 2D array for quality assurance. *The Egyptian Journal of Radiology and Nuclear Medicine, 49*(2), 477-484. doi:10.1016/j.ejrnm.2018.02.003

Moore, K. L. (2019). Automated Radiotherapy Treatment Planning. *Semin Radiat Oncol, 29*(3), 209-218. doi:10.1016/j.semradonc.2019.02.003

Morele, D., Gempp, S., Desrousseaux, J., Nigoul, J. M., & Capdeville, S. (2015). VMAT quality control implementation for an ELEKTA Beam Modulator accelerator, with Artiscan software. *Physica Medica, 31*. doi:10.1016/j.ejmp.2015.10.041

Muhammad, W., Maqbool, M., Shahid, M., Hussain, A., Tahir, S., Matiullah, . . . Lee, S. H. (2011). Assessment of computerized treatment planning system accuracy in calculating wedge factors of physical wedged fields for 6 MV photon beams. *Phys Med, 27*(3), 135-143. doi:10.1016/j.ejmp.2010.06.003

Natali, M., Capomolla, C., Russo, D., G, P., Cavalera, E., Leone, A., & Zagari, A. (2016). Dosimetric verificarion of vmat dose distribution with DELTA4 Phatom

Radioterapia.

Negri, A., Scaggion, A., Rossato, M. A., Canonico, D., Zandonà, R., & Paiusco, M. (2014). Evaluation of a phantom related gamma index threshold for VMAT QA. *Physica Medica, 30*. doi:10.1016/j.ejmp.2014.07.212

Nomden, C. N., Potter, R., de Leeuw, A. A. C., Tanderup, K., Lindegaard, J. C., Schmid, M. P., . . . Group, E. C. (2019). Nodal failure after chemo-radiation and MRI guided brachytherapy in cervical cancer: Patterns of failure in the EMBRACE study cohort. *Radiother Oncol, 134*, 185-190. doi:10.1016/j.radonc.2019.02.007

Onizuka, R., Araki, F., & Ohno, T. (2018). Monte Carlo dose verification of VMAT treatment plans using Elekta Agility 160-leaf MLC. *Physica Medica, 51*, 22-31. doi:10.1016/j.ejmp.2018.06.003

Orlandini, L. C., Betti, M., Fulcheri, C., Coppola, M., & Cionini, L. (2015). Dosimetric impact of different multileaf collimators on prostate intensity modulated treatment planning. *Rep Pract Oncol Radiother, 20*(5), 358-364. doi:10.1016/j.rpor.2015.06.005

Otto, K., Clark, C. H., Wood, K., Whitaker, S., & Nisbet, A. (2011). Volumetric modulated arc therapy: a review of current literature and clinical use in practice. *Br J Radiol, 84:967-96*.

Palisca, M. G., Eichler, T. J., & Hartford, A. C. (2009). American Society for Therapeutic Radiology and Oncology (ASTRO) and American College of Radiology (ACR)

practice guidelines for intensity modulated radiation therapy (IMRT). *Int J Radiat Oncol Biol Phys Med, 73(1):9e14*.

Park, J. M., Kim, D. I., Kim, J. I., & Yoo, S. H. (2013). Study on monitoring unit efficiency of flattening-filter free photon beam in association with tumor size and location. . *J Radiat Protect*

38.

Pecorelli, S., & (2009). Revised FIGO for carcinoma of the vulva, cervix, and endometrium. *International Journal of Gynecology and Obstetrics, 105(2):103(4)*.

Petric, P., Hudej, R., Marolt-Mušič , M., & 2009;. (2009). MRI assisted cervix cancer brachytherapy pre-planning, based on insertion of the applicator in para- cervical anaesthesia: preliminary results of a prospective study. . *J Contemp Brachyther., 1(3):163-169*.

Podgoršak, E. B. (2005). Radiation oncology physics : a handbook for teachers and students.

. *International Atomic Energy Agency*.

Poon, I., Xia, P., Weinberg, V., Sultanem, K., Akazawa, C., Akazawa, P., . . . Lee, N. (2007). A treatment planning analysis of inverse-planned and forward-planned intensity-modulated radiation therapy in nasopharyngeal carcinoma. *Int J Radiat Oncol Biol Phys, 69*(5), 1625-1633. doi:10.1016/j.ijrobp.2007.08.028

Pötter, R., Dimopoulos, J., Kirisits, C., Lang, S., Haie-Meder, C., Briot, E., . . . Petrow, P. (2005). Recommendations for image-based intracavitary brachytherapy of cervix cancer: the GYN GEC ESTRO Working Group point of view: in regard to Nag et al. *Int J Radiat Oncol Biol Phys, 62(1):293-5*.

Qiu, J. J., Chang, Z., & Wu, Q. J. (2010). Impact of volumetric modulated arc therapy technique on treatment with partial breast irradiation. *Int. J. Radiat. Oncol. Biol. Phys., 78 (1), 288–296*.

Ramtohul, M., Ford, D., Cashmore, J., & (2011). Lowering whole-body doses in pediatric intensity-modulated radiotherapy through the use of unflattened photon beams. *Int J Radiat Oncol Biol Phys*

80(July (4)):1220–7.

Reynaert, N., van der Marck, S. C., Schaart, D. R., Van der Zee, W., Van Vliet-Vroegindeweij, C., Tomsej, M., . . . De Wagter, C. (2007). Monte Carlo treatment planning for photon and electron beams. *Radiation Physics and Chemistry, 76*(4), 643-686. doi:10.1016/j.radphyschem.2006.05.015

Rothman, J., Greenland, S., & Lash, T. (2008). Modern Epidemiology. *Lippincott Williams & Wilkins*

3rd Edition.

Rout, B. K., Muralidhar, K. R., Ali, M., & Shekar, M. C. (2014). Dosimetric study of RapidArc plans with flattened beam (FB) and flattening filter-free (FFF) beam for localized prostate cancer based on physical indices. *Int J Cancer Ther Oncol, 2(4):02046*.

Sannazzari, G. L., Ragona, R., & Ruo, R. M. G. (2002). CT-MRI image fusion for delineation of volumes in three dimensional conformal radiation therapy in the treatment of localized prostate cancer. *Br J Radiol, 75:603-7*.

Sasaoka, M., Futami, T., breast, D. e. o. w., radiotherapy using field in field technique in early breast cancer, I., & 16:250-256., J. C. O. (2011). Dosimetric evaluation of

whole breast radiotherapy using field in field technique in early breast cancer,. *Int J Clin Oncol, 16:250-256.*

Serban, M., Kirisits, C., Potter, R., de Leeuw, A., Nkiwane, K., Dumas, I., . . . Group, E. C. (2018). Isodose surface volumes in cervix cancer brachytherapy: Change of practice from standard (Point A) to individualized image guided adaptive (EMBRACE I) brachytherapy. *Radiother Oncol, 129*(3), 567-574. doi:10.1016/j.radonc.2018.09.002

Shaffer, R., Nichol, A. M., & Vollans, E. (2009). A comparison of volumetric modulated arc therapy and conventional intensity-modulated radiotherapy for frontal and temporal high-grade gliomas. . *Int. J. Radiat. Oncol. Biol. Phys, 76 (4),1177–1184.*

.

Sharfo, A. W., Voet, P. W., Breedveld, S., Mens, J. W., Hoogeman, M. S., & Heijmen, B. J. (2015). Comparison of VMAT and IMRT strategies for cervical cancer patients using automated planning. *Radiother Oncol, 114*(3), 395-401. doi:10.1016/j.radonc.2015.02.006

Sharma, S. D., & (2011). Unflattened photon beams from the standard flattening filter free accelerators for radiotherapy: advantages, limitations and challenges. *J Appl Clin Med Phys, 123-5*.

Small, W. J., Bacon, M. A., Bajaj, A., & (2017). Cervical cancer: a global health crisis. *123: 2404–12.*

Stathakis, S., Mavroidis, P., Shi, C., Xu, J., Kauweloa, K. I., Narayanasamy, G., & Papanikolaou, N. (2014). gamma+ index: A new evaluation parameter for

quantitative quality assurance. *Comput Methods Programs Biomed, 114*(1), 60-69. doi:10.1016/j.cmpb.2014.01.005

Suresh, T., Madeswaran, S., Anjali, P., & Abhinav, D. (2018). Comparative Evaluation of a 6MV Flattened Beam and a Flattening Filter Free Beam for Carcinoma of Cervix – IMRT Planning Study. *Asian Pacific Journal of Cancer Prevention, 19:639*. doi:DOI:10.22034/APJCP.2018.19.3.639

Tan, L. T., Tanderup, K., Hoskin, P., Cooper, R., & Potter, R. (2018). Image-guided Adaptive Brachytherapy for Cervix Cancer - A Story of Successful Collaboration within the GEC-ESTRO GYN Network and the EMBRACE Studies. *Clin Oncol (R Coll Radiol), 30*(7), 397-399. doi:10.1016/j.clon.2018.04.005

Taylor, A., Rockall, A. G., Reznek, R. H., Powell, M. E., & (2005). Mapping pelvic lymph nodes: guidelines for delineation in intensity-modulated radiotherapy. *Int J Radiat Oncol Biol Phys, 63(5):1604-1612.*

.

Thwaites, D., & Tuohy, J. B. (2006). Back to the future: the history and development of the clinical linear accelerator *Phys Med Biol, 51 (2006) R343–R362*

Titt, U., Vassiliev, O. N., Pönisch, F., Dong, L., Liu, H., & Mohan, R. A. (2006). flattening filter free photon treatment concept evaluation with Monte Carlo. . *Med Phys, 33*.

Troost, E., Thorwarth, D., & Oyen, W. (2015). Imaging-based treatment adaptation in radiation oncology. *J Nucl Med, 56:1922*.

Verbakel, W. F. A. R., Cuijpers, J. P., Hoffmans, D., Bieker, M., Slotman, B. J., & Senan, S. (2009). Volumetric intensity-modulated arc therapy vs. conventional IMRT in headand-neck cancer: a comparative planning and dosimetric study. *Int J Radiat*

Oncol Biol Phys 74:252e9.

White, P. (2017). Comparing Two Samples from an Individual Likert Question. *International Journal of Mathematics and Statistics, 18 (3): 1–13*.

Williams, J. R., Thwaites, D. I., & (2000). Radiotherapy Physics in Practice,. *Oxford Univ. Press*.

Wolfsberger, L., Wagar, M., Nitsch, P., Bhagwat, M., & Zygmanski, P. (2010). Angular dose dependence of Matrixx TM and its calibration. . *J Appl Clin Med Phys, 11(1)*.

Xing, A., Arumugam, S., Deshpande, S., George, A., Vial, P., Holloway, L., & Goozee, G. (2015). Evaluation of 3D Gamma index calculation implemented in two commercial dosimetry systems. *Journal of Physics: Conference Series, 573*. doi:10.1088/1742-6596/573/1/012054

Yamazaki, A., Shirato, H., & Nishioka, T. (2000). Reduction of late complications after irregularly shaped four-field whole pelvic radiotherapy using computed tomographic simulation compared with parallel-opposed whole pelvic radiotherapy. *J Clin Oncol 30:180e184.*

Yoo, S. (2010). Radiotherapy treatment plans with RapidArc for prostate cancer involving seminal vescicles and lymph nodes. *Int J Radiat Oncol Biol Phys, 76:935-42*.

Yu, C. X., & Tang, G. (2011). Intensity-modulated arc therapy: principles, technologies and clinical implementation. *Phys Med Biol., 56(5):R31–54*.

Zivanovic, O., Alektiar, K. M., Sonoda, Y., Zhou, Q., Iasonos, A., Tew, W. P., . . . Abu-Rustum, N. R. (2008). Treatment patterns of FIGO Stage IB2 cervical cancer: a single-institution experience of radical hysterectomy with individualized

postoperative therapy and definitive radiation therapy. *Gynecol Oncol, 111*(2), 265-270. doi:10.1016/j.ygyno.2008.07.050

APPENDIX

APPENDIX 1

Table A.1: Factor of the day for 6MVand FFF plans

Linac	6MV	FFF
SB3	1.0387	1.0331
SB5	1.042	1. 0386
SB6	1.0439	1.0422

Table A.2: Gamma pass rates before machine optimization [SB3]

	6MV			FFF		
Patient	arc1 [%]	arc2 [%]	Total [%]	arc3 [%]	arc4 [%]	Total [%]
PT1	99.4	100.0	99.9	93.5	81.4	78.3
PT2	100.0	97.1	99.1	96.5	98.0	95.6
PT3	100.0	96.2	96.1	94.8	91.8	84.8
PT4	100.0	93.1	98.6	97.8	98.0	88.9
PT5	98.8	99.4	99.4	96.7	98.0	97.2
PT6	98.9	97.7	99.1	98.1	93.1	86.5
PT7	100.0	100.0	100.0	93.4	99.1	95.6
PT8	99.4	98.9	100.0	95.3	98.1	96.2
PT9	99.0	99.7	99.1	98.1	99.0	92.5
PT10	98.6	97.0	96.0	84.9	91.6	83.8
PT11	97.4	90.3	93.9	70.7	99.5	82.0
PT12	0.0	0.0	0.0	91.0	93.1	78.2
PT13	99.6	99.1	99.1	91.3	97.8	87.3
PT14	100.0	96.7	100.0	97.9	99.1	99.5
PT15	97.1	99.8	98.3	95.9	98.1	96.5

Table A.3: Gamma pass rates after machine optimization [SB3]

	6MV			FFF		
Patient	arc1 [%]	arc2 [%]	Total [%]	arc3 [%]	arc4 [%]	Total [%]
PT1	99.8	98.6	98.9	98.9	86.6	85.6
PT2	100.0	97.7	99.4	96.3	98.0	95.6
PT3	99.8	99.1	98.9	95.2	91.1	83.5
PT4	99.8	99.9	100.0	99.4	98.7	92.7
PT5	99.7	99.9	100.0	99.3	99.3	99.1
PT6	99.8	99.4	99.8	99.2	95.0	92.3
PT7	99.7	100.0	100.0	95.2	99.0	97.9
PT8	99.7	99.7	100.0	96.2	98.6	94.6
PT9	99.5	100.0	99.9	98.7	99.8	93.9
PT10	99.7	98.8	98.8	93.7	93.8	94.8
PT11	98.7	92.5	98.7	92.2	100.0	92.4
PT12	0.0	0.0	0.0	93.0	99.6	94.6
PT13	100.0	99.6	99.9	94.8	100.0	95.6
PT14	100.0	99.6	100.0	99.2	100.0	99.7
PT15	99.6	99.8	99.4	98.6	95.3	84.6

Table A.4: Gamma pass rates before machine optimization [SB5]

	6MV			FFF		
Patient	arc1 [%]	arc2 [%]	Total [%]	arc3 [%]	arc4 [%]	Total [%]
PT1	98.7	99.8	99.0	94.6	91.2	88.6
PT2	100.0	96.1	99.5	95.0	98.2	95.9
PT3	99.8	97.9	99.2	91.4	93.3	86.1
PT4	99.6	93.5	99.1	98.3	98.7	94.2
PT5	98.8	99.4	99.4	96.7	98.0	97.2
PT6	98.9	98.6	99.4	97.4	93.6	88.9
PT7	99.9	99.5	100.0	93.5	98.7	96.7
PT8	99.7	97.6	100.0	95.1	97.9	93.6
PT9	99.0	99.7	99.2	98.1	99.8	94.7
PT10	95.1	98.2	95.4	90.5	94.8	90.8
PT11	96.1	91.9	94.3	69.9	99.5	90.6
PT12	98.8	98.8	98.6	90.4	95.3	83.0
PT13	99.6	98.9	99.1	92.9	98.4	92.2
PT14	100.0	97.5	99.7	97.1	98.4	99.1
PT15	97.9	99.3	99.0	98.6	94.8	84.3

Table A.5: Gamma pass rates after machine optimization [SB5]

	6MV			FFF		
Patient	arc1 [%]	arc2 [%]	Total [%]	arc3 [%]	arc4 [%]	Total [%]
PT1	100.0	100.0	100.0	99.7	97.8	97.0
PT2	99.8	100.0	100.0	100.0	99.8	100.0
PT3	100.0	99.8	100.0	99.8	99.8	99.8
PT4	99.8	100.0	100.0	100.0	100.0	98.4
PT5	100.0	100.0	100.0	100.0	100.0	99.9
PT6	100.0	99.7	100.0	100.0	99.8	99.5
PT7	99.9	100.0	100.0	99.8	99.8	99.9
PT8	100.0	100.0	100.0	99.4	99.5	100.0
PT9	100.0	100.0	100.0	100.0	100.0	99.4
PT10	100.0	100.0	99.6	97.8	98.3	96.8
PT11	100.0	99.4	100.0	100.0	100.0	99.6
PT12	100.0	100.0	100.0	99.1	99.3	95.4
PT13	100.0	100.0	100.0	92.9	98.4	92.2
PT14	100.0	100.0	100.0	100.0	100.0	100.0
PT15	100.0	100.0	100.0	98.5	99.5	98.8

Table A.6: Gamma pass rates [SB6]

	6MV			FFF		
Patient	arc1 [%]	arc2 [%]	Total [%]	arc3 [%]	arc4 [%]	Total [%]
PT1	99.3	100.0	99.0	97.0	90.4	90.0
PT2	100.0	99.0	100.0	99.6	98.2	98.2
PT3	100.0	99.8	99.8	100.0	96.3	98.9
PT4	100.0	99.0	99.6	95.5	96.8	94.6
PT5	99.9	99.7	99.7	99.5	97.8	96.5
PT6	100.0	98.3	99.4	100.0	99.5	98.0
PT7	99.6	100.0	99.9	97.9	98.6	95.4
PT8	99.8	100.0	100.0	99.2	97.8	98.0
PT9	97.0	99.8	99.7	99.4	99.0	96.2
PT10	100.0	99.4	99.7	94.4	94.6	92.3
PT11	100.0	95.3	97.8	95.1	96.4	97.9
PT12	100.0	99.7	100.0	98.8	94.2	90.7
PT13	100.0	99.8	100.0	98.2	99.4	98.1
PT14	100.0	100.0	100.0	99.5	98.8	97.9
PT15	99.6	100.0	99.4	98.5	98.5	97.7

Table A.7: Monitor units for 6MV and FFF plans

	6MV			FFF		
Patient	arc1	arc2	Total	arc3	arc4	Total
PT1	274.7	254.7	529.4	364.8	452.0	816.8
PT2	232.3	282.3	514.6	272.4	539.2	811.6
PT3	178.0	224.8	402.8	229.5	285.7	515.2
PT4	220.5	272.1	492.6	401.6	326.4	728.0
PT5	202.3	333.7	536.0	275.1	364.2	639.3
PT6	184.3	252.1	436.4	315.5	321.7	637.2
PT7	223.5	220.9	444.4	341.0	368.1	709.1
PT8	175.5	321.0	496.5	306.5	409.7	716.2
PT9	269.7	313.7	583.4	351.3	389.2	740.5
PT10	283.1	311.2	594.3	360.4	487.3	847.7
PT11	249.7	338.8	588.5	327.6	371.4	699.0
PT12	225.5	282.0	507.5	416.8	334.4	751.2
PT13	229.5	262.1	491.6	282.9	308.9	591.8
PT14	237.9	246.2	484.1	294.3	304.4	598.7
PT15	268.3	266.4	534.7	311.5	348.7	660.2

Table A.8: Volume of PTV

Patient	PTV[cm^3]
PT1	2011.54
PT2	1787.56
PT3	1957.08
PT4	2209.12
PT5	2212.21
PT6	1426.20
PT7	2546.02
PT8	1967.47
PT9	2002.40
PT10	1741.75
PT11	2193.84
PT12	1828.56
PT13	1040.70
PT14	2023.31
PT15	1610.81

APPENDIX 2

MATLAB CODES

```
% loading data from SB3
% data for 6MV before and after machine optimization
MVbef_3 = readtable(fullfile('C:\Users\admin\OneDrive\master
thesis\sb3','sb3.6MV_bef.xlsx'));
MVaft_3 = readtable(fullfile('C:\Users\admin\OneDrive\master
thesis\sb3','sb3.6MV_aft.xlsx'));

% data for FFF before and after machine optimization
FFFbef_3 = readtable(fullfile('C:\Users\admin\OneDrive\master
thesis\sb3','sb3.FFF_bef.xlsx'));
FFFaft_3 = readtable(fullfile('C:\Users\admin\OneDrive\master
thesis\sb3','sb3.FFF_aft.xlsx'));

% loading data from SB5
% data for 6MV before and after machine optimization
MVbef_5 = readtable(fullfile('C:\Users\admin\OneDrive\master
thesis\sb5','sb5.6MV_bef19.xlsx'));
MVaft_5 = readtable(fullfile('C:\Users\admin\OneDrive\master
thesis\sb5','sb5.6MV_aft19.xlsx'));

% data for FFF before and after machine optimization
FFFbef_5 = readtable(fullfile('C:\Users\admin\OneDrive\master
thesis\sb5','sb5.FFF_bef19.xlsx'));
FFFaft_5 = readtable(fullfile('C:\Users\admin\OneDrive\master
thesis\sb5','sb5.FFF_aft19.xlsx'));
```

```
% loading data for SB5 2018
MV_sb5_18 = readtable(fullfile('C:\Users\admin\OneDrive\master
thesis\sb5','sb5.6MV_18.xlsx'));
FFF_sb5_18 = readtable(fullfile('C:\Users\admin\OneDrive\master
thesis\sb5','sb5.FFF_18.xlsx'));

% loading data from SB6
MV_sb6 = readtable(fullfile('C:\Users\admin\OneDrive\master
thesis\sb6','sb6.6MV.xlsx'));
FFF_sb6 = readtable(fullfile('C:\Users\admin\OneDrive\master
thesis\sb6','sb6.FFF.xlsx'));

%calculating mean passrate and std for 6MV sb3 before optimization
mean_MVbef_3_arc1 = mean(MVbef_3.x_PassRateArc1);
mean_MVbef_3_arc2 = mean(MVbef_3.x_PassRateArc2);
mean_MVbef_3_total = mean(MVbef_3.Total_PassRate);

std_MVbef_3_arc1 = std(MVbef_3.x_PassRateArc1);
std_MVbef_3_arc2 = std(MVbef_3.x_PassRateArc2);
std_MVbef_3_total = std(MVbef_3.Total_PassRate);

%calculating mean passrate and std for 6MV sb3 after optimization
mean_MVaft_3_arc1 = mean(MVaft_3.x_PassRateArc1);
mean_MVaft_3_arc2 = mean(MVaft_3.x_PassRateArc2);
mean_MVaft_3_total = mean(MVaft_3.Total_PassRate);
```

```
std_MVaft_3_arc1 = std(MVaft_3.x_PassRateArc1);
std_MVaft_3_arc2 = std(MVaft_3.x_PassRateArc2);
std_MVaft_3_total = std(MVaft_3.Total_PassRate);

%calculating mean passrate and std for FFF sb3 before optimization
mean_FFFbef_3_arc3 = mean(FFFbef_3.x_PassRateArc3);
mean_FFFbef_3_arc4 = mean(FFFbef_3.x_PassRateArc4);
mean_FFFbef_3_total = mean(FFFbef_3.Total_PassRate);

std_FFFbef_3_arc3 = std(FFFbef_3.x_PassRateArc3);
std_FFFbef_3_arc4 = std(FFFbef_3.x_PassRateArc4);
std_FFFbef_3_total = std(FFFbef_3.Total_PassRate);

%calculating mean passrate and std for FFF sb3 after optimization
mean_FFFaft_3_arc3 = mean(FFFaft_3.x_PassRateArc3);
mean_FFFaft_3_arc4 = mean(FFFaft_3.x_PassRateArc4);
mean_FFFaft_3_total = mean(FFFaft_3.Total_PassRate);

std_FFFaft_3_arc3 = std(FFFaft_3.x_PassRateArc3);
std_FFFaft_3_arc4 = std(FFFaft_3.x_PassRateArc4);
std_FFFaft_3_total = std(FFFaft_3.Total_PassRate);

%calculating mean passrate and std for 6MV sb5 before optimization
mean_MVbef_5_arc1 = mean(MVbef_5.x_PassRateArc1);
mean_MVbef_5_arc2 = mean(MVbef_5.x_PassRateArc2);
mean_MVbef_5_total = mean(MVbef_5.Total_PassRate);
```

```
std_MVbef_5_arc1 = std(MVbef_5.x_PassRateArc1);
std_MVbef_5_arc2 = std(MVbef_5.x_PassRateArc2);
std_MVbef_5_total = std(MVbef_5.Total_PassRate);

%calculating mean passrate and std for 6MV sb5 after optimization
mean_MVaft_5_arc1 = mean(MVaft_5.x_PassRateArc1);
mean_MVaft_5_arc2 = mean(MVaft_5.x_PassRateArc2);
mean_MVaft_5_total = mean(MVaft_5.Total_PassRate);

std_MVaft_5_arc1 = std(MVaft_5.x_PassRateArc1);
std_MVaft_5_arc2 = std(MVaft_5.x_PassRateArc2);
std_MVaft_5_total = std(MVaft_5.Total_PassRate);

%calculating mean passrate and std for FFF sb5 before optimization
mean_FFFbef_5_arc3 = mean(FFFbef_5.x_PassRateArc3);
mean_FFFbef_5_arc4 = mean(FFFbef_5.x_PassRateArc4);
mean_FFFbef_5_total = mean(FFFbef_5.Total_PassRate);

std_FFFbef_5_arc3 = std(FFFbef_5.x_PassRateArc3);
std_FFFbef_5_arc4 = std(FFFbef_5.x_PassRateArc4);
std_FFFbef_5_total = std(FFFbef_5.Total_PassRate);

%calculating mean passrate and std for FFF sb5 after optimization
mean_FFFaft_5_arc3 = mean(FFFaft_5.x_PassRateArc3);
mean_FFFaft_5_arc4 = mean(FFFaft_5.x_PassRateArc4);
mean_FFFaft_5_total = mean(FFFaft_5.Total_PassRate);
```

```
std_FFFaft_5_arc3 = std(FFFaft_5.x_PassRateArc3);
std_FFFaft_5_arc4 = std(FFFaft_5.x_PassRateArc4);
std_FFFaft_5_total = std(FFFaft_5.Total_PassRate);

% calculating mean passrate and std for 6MV sb5 2018
mean_MV_sb5_18_arc1 = mean(MV_sb5_18.x_PassRateArc1);
mean_MV_sb5_18_arc2 = mean(MV_sb5_18.x_PassRateArc2);
mean_MV_sb5_18_total = mean(MV_sb5_18.Total_PassRate);

std_MV_sb5_18_arc1 = std(MV_sb5_18.x_PassRateArc1);
std_MV_sb5_18_arc2 = std(MV_sb5_18.x_PassRateArc2);
std_MV_sb5_18_total = std(MV_sb5_18.Total_PassRate);

% calculating mean passrate and std for FFF sb5 2018
mean_FFF_sb5_18_arc3 = mean(FFF_sb5_18.x_PassRateArc3);
mean_FFF_sb5_18_arc4 = mean(FFF_sb5_18.x_PassRateArc4);
mean_FFF_sb5_18_total = mean(FFF_sb5_18.Total_PassRate);

std_FFF_sb5_18_arc3 = std(FFF_sb5_18.x_PassRateArc3);
std_FFF_sb5_18_arc4 = std(FFF_sb5_18.x_PassRateArc4);
std_FFF_sb5_18_total = std(FFF_sb5_18.Total_PassRate);

% calculating mean passrate and std for 6MV sb6
mean_MV_sb6_arc1 = mean(MV_sb6.x_PassRateArc1);
mean_MV_sb6_arc2 = mean(MV_sb6.x_PassRateArc2);
mean_MV_sb6_total = mean(MV_sb6.Total_PassRate);
```

```
std_MV_sb6_arc1 = std(MV_sb6.x_PassRateArc1);
std_MV_sb6_arc2 = std(MV_sb6.x_PassRateArc2);
std_MV_sb6_total = std(MV_sb6.Total_PassRate);

% calculating mean passrate and std for FFF sb6
mean_FFF_sb6_arc3 = mean(FFF_sb6.x_PassRateArc3);
mean_FFF_sb6_arc4 = mean(FFF_sb6.x_PassRateArc4);
mean_FFF_sb6_total = mean(FFF_sb6.Total_PassRate);

std_FFF_sb6_arc3 = std(FFF_sb6.x_PassRateArc3);
std_FFF_sb6_arc4 = std(FFF_sb6.x_PassRateArc4);
std_FFF_sb6_total = std(FFF_sb6.Total_PassRate);

% plotting a graph of the passrates of 6MV and FFF beams for SB3 before
and after machine optimization
figure();
boxplot([MVbef_3.Total_PassRate,FFFbef_3.Total_PassRate],{'6MV','FFF'})
;
title('Gamma Pass rates before optimization [SB3]');
xlabel('');
ylabel('pass rates [%]');
ylim([75 105]);
signrank(MVbef_3.Total_PassRate,FFFbef_3.Total_PassRate); % Wilcoxon
test for SB3 before optimization


figure();
```

```
boxplot([MVaft_3.Total_PassRate,FFFaft_3.Total_PassRate],{'6MV','FFF'})
;
title('Gamma Pass rates after optimization [SB3]');
xlabel('');
ylabel('pass rates [%]');
ylim([75 105]);
signrank(MVaft_3.Total_PassRate,FFFaft_3.Total_PassRate); % Wilcoxon
test for SB3 after optimization



% plotting a graph of the passrates of 6MV and FFF beams for SB5 before
and after machine optimization
figure();
boxplot([MVbef_5.Total_PassRate,FFFbef_5.Total_PassRate],{'6MV','FFF'})
;
title('Gamma Pass rates before optimization [SB5]');
xlabel('');
ylabel('pass rates [%]');
ylim([75 105]);
signrank(MVbef_5.Total_PassRate,FFFbef_5.Total_PassRate); % Wilcoxon
test for SB5 before optimization



figure();
boxplot([MVaft_5.Total_PassRate,FFFaft_5.Total_PassRate],{'6MV','FFF'})
;
title('Gamma Pass rates after optimization [SB5]');
xlabel('');
```

```
ylabel('pass rates [%]');
ylim([75 105]);
signrank(MVaft_5.Total_PassRate,FFFaft_5.Total_PassRate); % Wilcoxon
test for SB5 after optimization



figure();
boxplot([MV_sb6.Total_PassRate,FFF_sb6.Total_PassRate],{'6MV','FFF'});
title('Gamma Pass rates [SB6]');
xlabel('');
ylabel('pass rates [%]');
ylim([75 105]);
signrank(MV_sb6.Total_PassRate,FFF_sb6.Total_PassRate); % Wilcoxon test
for SB6



figure();
boxplot([MV_sb5_18.Total_PassRate,MVbef_5.Total_PassRate,FFF_sb5_18.Tot
al_PassRate,FFFbef_5.Total_PassRate],{'6MV [2018]','6MV','FFF
[2018]','FFF'});
title('Gamma Pass rates  [SB5,2018 vs 2019]');
xlabel('');
ylabel('pass rates [%]');
ylim([75 105]);
signrank(MV_sb5_18.Total_PassRate,MVbef_5.Total_PassRate); % Wilcoxon
test for 6MV 2018 and current data (SB5)
signrank(FFF_sb5_18.Total_PassRate,FFFbef_5.Total_PassRate); % Wilcoxon
test for FFF 2018 and current data
```

```
% comparison of the gamma pass rate for all 3 linacs [ SB3, SB5 &
SB6]6MV
figure();
boxplot([MVaft_3.Total_PassRate,MVaft_5.Total_PassRate,MV_sb6.Total_Pas
sRate],{'6MV [SB3]','6MV [SB5]','6MV [SB6]'});
title('Gamma Pass rates for 6MV  [SB3,SB5 & SB6]');
xlabel('');
ylabel('pass rates [%]');
ylim([75 105]);
signrank(MVaft_3.Total_PassRate,MVaft_5.Total_PassRate); % Wilcoxon
test for SB3 & SB5
signrank(MVaft_3.Total_PassRate,MV_sb6.Total_PassRate); % Wilcoxon test
for SB3 & SB6
signrank(MVaft_5.Total_PassRate,MV_sb6.Total_PassRate); % Wilcoxon test
for SB5 & SB6



% comparison of the gamma pass rate for all 3 linacs [ SB3, SB5 &
SB6]FFF
figure();
boxplot([FFFaft_3.Total_PassRate,FFFaft_5.Total_PassRate,FFF_sb6.Total_
PassRate],{'FFF [SB3]','FFF [SB5]','FFF [SB6]'});
title('Gamma Pass rates for FFF  [SB3,SB5 & SB6]');
xlabel('');
ylabel('pass rates [%]');
ylim([75 105]);
```

```
signrank(FFFaft_3.Total_PassRate,FFFaft_5.Total_PassRate); % Wilcoxon
test for SB3 & SB5
signrank(FFFaft_3.Total_PassRate,FFF_sb6.Total_PassRate); % Wilcoxon
test for SB3 & SB6
signrank(FFFaft_5.Total_PassRate,FFF_sb6.Total_PassRate); % Wilcoxon
test for SB5 & SB6



% individual gamma pass rate for both 6MV and FFF using SB3
figure();
barh([MVaft_3.Total_PassRate,FFFaft_3.Total_PassRate]);
title('Individual gamma pass rates SB3');
xlabel('Pass rate [%]');
ylabel('Patient number');
legend('6MV','FFF');
xlim([80 105]);



% individual gamma pass rate for both 6MV and FFF using SB5
figure();
barh([MVaft_5.Total_PassRate,FFFaft_5.Total_PassRate]);
title('Individual gamma pass rates SB5');
xlabel('Pass rate [%]');
ylabel('Patient number');
legend('6MV','FFF');
xlim([80 105]);
```

```
% individual gamma pass rate for both 6MV and FFF using SB6
figure();
barh([MV_sb6.Total_PassRate,FFF_sb6.Total_PassRate]);
title('Individual gamma pass rates SB6');
xlabel('Pass rate [%]');
ylabel('Patient number');
legend('6MV','FFF');
xlim([80 105]);



% monitor unit
mean(MVaft_5.TotalMonitorUnit);
std(MVaft_5.TotalMonitorUnit);
mean(FFFaft_5.TotalMonitorUnit);
std(FFFaft_5.TotalMonitorUnit);

figure();
boxplot([MVaft_5.TotalMonitorUnit,FFFaft_5.TotalMonitorUnit],{'6MV','FF
F'});
title('Monitor units for 6MV & FFF beams');
xlabel('');
ylabel('MUs');
ylim([400 900]);
signrank(MVaft_5.TotalMonitorUnit,FFFaft_5.TotalMonitorUnit); %
Wilcoxon test for monitor unit



% scatter plot of 6MV vs FFF
```

```
figure();
scatter(MVaft_5.TotalMonitorUnit,FFFaft_5.TotalMonitorUnit,'r','bl')
title('Monitor units [6MV vs FFF]');
xlabel('6MV');
ylabel('FFF');
axis([375 900 375 900]);
refline(1,0); % constructing reference unity line



% monitor units and pass rate
pf1 = polyfit(MVaft_5.TotalMonitorUnit,MVaft_5.Total_PassRate,1);
pv1 = polyval(pf1,MVaft_5.TotalMonitorUnit);
pf2 = polyfit(FFFaft_5.TotalMonitorUnit,FFFaft_5.Total_PassRate,1);
pv2 = polyval(pf2,FFFaft_5.TotalMonitorUnit);


% making plots with trend line
figure();
scatter(MVaft_5.TotalMonitorUnit,MVaft_5.Total_PassRate,'bl','*');
title('Total MU vs total pass rate');
xlabel('MUs');
ylabel('Pass rate [%]');
hold on
scatter(FFFaft_5.TotalMonitorUnit,FFFaft_5.Total_PassRate,'r','*');
hold on
plot(MVaft_5.TotalMonitorUnit,pv1,'-');
hold on
plot(FFFaft_5.TotalMonitorUnit,pv2,'-');
axis([350 900 90 105]);
```

```
legend('6MV','FFF','Trend line 6MV','Trend line FFF');


% volume of PTV and gamma pass rate
pff1 = polyfit(MVaft_5.VolumeOfPTV_cm3_,MVaft_5.Total_PassRate,1);
pvv1 = polyval(pff1,MVaft_5.VolumeOfPTV_cm3_);
pff2 = polyfit(FFFaft_5.VolumeOfPTV,FFFaft_5.Total_PassRate,1);
pvv2 = polyval(pff2,FFFaft_5.VolumeOfPTV);


figure();
scatter(MVaft_5.VolumeOfPTV_cm3_,MVaft_5.Total_PassRate,'bl','*');
title('PTV volume vs Pass rate');
xlabel('PTV volume [cm^3]');
ylabel('Pass rate [%]');
axis([1000 2600 90 105]);
hold on
scatter(FFFaft_5.VolumeOfPTV,FFFaft_5.Total_PassRate,'r','*');
hold on
plot(MVaft_5.VolumeOfPTV_cm3_,pvv1,'-');
hold on
plot(FFFaft_5.VolumeOfPTV,pvv2,'-');
legend('6MV','FFF','Trend line 6MV','Trend line FFF');


% analysis of median values for 6MV and FFF (SB5)
mean(MVaft_5.TotalMedian___);
std(MVaft_5.TotalMedian___);
mean(FFFaft_5.TotalMedian___);
std(FFFaft_5.TotalMedian___);
scatter(MVaft_5.TotalMedian___,FFFaft_5.TotalMedian___,'r','*');
```